Executive Summary

CRITICAL PARAMETERS FOR CORROSION INDUCED DETERIORATION OF MARINE BRIDGE SUBSTRUCTURES IN FLORIDA

(BD-166)

submitted to

Florida Department of Transportation Research Center
605 Suwannee Street
Tallahassee, Florida 32399

submitted by

William H. Hartt and Jingak Nam,
Center for Marine Materials
Department of Ocean Engineering
Florida Atlantic University – Sea Tech Campus
101 North Beach Road
Dania Beach, Florida 33004

April 9, 2004

EXECUTIVE SUMMARY

Improving upon methods and procedures for addressing corrosion induced deterioration of Florida coastal bridge substructures continues to be an objective of the Florida Department of Transportation. The research performed in this project addressed this concern based upon the premise that concretes formulated using high alkalinity cements (equivalent alkalinity, Na_2O_e, ~ 1.00) can provide enhanced corrosion resistance to embedded reinforcement compared to ones of normal alkalinity (Na_2O_e < 0.60) by elevating the critical threshold concentration of chlorides required for breakdown of passivity and initiation of active corrosion. To accomplish this, experiments were performed where time-to-corrosion initiation of both G109 and simulated piling specimens was monitored. The former type specimens (G109s) were exposed to cyclic wet-dry ponding with a 15 weight percent (w/o) NaCl solution, and time-to-corrosion was monitored using potential and macrocell current measurements. Mix design variables included cement alkalinity (Na_2O_e = 1.078 (high) and 0.317 (low)) and water cement ratio (0.50 and 0.37), and bar surface condition was either as received or wire brushed. Subsequent to corrosion initiation, specimens were autopsied and determinations made of the critical chloride concentration for corrosion initiation. The latter specimens (simulated piling type) were continuously exposed, partially submerged in 15 w/o NaCl and potential monitored to determine the onset of corrosion. Data for both specimen types were represented using Weibull statistics. This revealed that the mean chloride threshold for even the low Na_2O_e specimens exceeded what has historically been reported for bridge substructures in Florida (1.2-3.5 kg/m^3 (2-6 pcy)) by a factor of 1.5-8. At the same time, however, the chloride threshold for corrosion initiation with a 1-10 percent probability of occurrence was in the range of the Florida experience. Time-to-corrosion for the high alkalinity specimens exceeded that for the low alkalinity ones by a factor of from two to six, thus confirming an advantage from the corrosion standpoint of employing cements in this category. A preferential tendency for corrosion to initiate at relatively large air voids (diameters 3-5 mm) was disclosed. This indicates that time-to-corrosion can be additionally forestalled if methods can be practiced that reduce the size and density of air voids in concretes that are delivered to job sites.

In addition, exposures of non-reinforced concrete specimens were conducted in 1) constant relative humidity chambers (RH = 35, 55, 75, and 95 percent), in which specimens were sprayed with a 15 w/o NaCl solution on alternate days, and 2) constant temperature chambers (0, 30, and 40^{o}C) and in the ambient laboratory environment (temperature ~ 23^{o}C) with continuous ponding with 15 w/o NaCl. Data from these experiments indicated that the effective Cl^- diffusion coefficient, D_{eff}, increased with increasing RH and with increasing temperature. Results of an experiment where a specimen was cycled between RH 35 and 95 percent indicated that D_{eff} was approximately that of the mid-RH value (65 percent). This suggests that Cl^- ingress rates that occur in actual exposures, where RH is variable, can be projected from laboratory exposures performed at constant RH. However, results of an experiment where a specimen was cycled between 23 and 40^{o}C showed that D_{eff} was greater than at even 40^{o}C. This indicates that caution should be exercised in projecting chloride ingress rate for actual structures based upon laboratory experiments performed at constant temperature.

TABLE OF CONTENTS

LIST OF TABLES

LIST OF FIGURES

Page

INTRODUCTION

Overview of Concrete Deterioration Processes

General

While concrete has evolved to become the most widely used structural material in the world, the fact that its capacity for plastic deformation is essentially nil imposes major practical design limitations. This shortcoming is most commonly overcome by incorporation of steel reinforcement into those locations in the concrete where tensile stresses are anticipated. Consequently, concerns regarding performance must not only focus upon properties of the concrete itself but also of the embedded steel and, in addition, the manner in which these two components interact. In this regard, steel and concrete are in most aspects mutually compatible, as exemplified by the fact that the coefficient of thermal expansion for each is approximately the same. Also, while boldly exposed steel corrodes actively in most natural environments at a rate that requires use of extrinsic corrosion control measures (for example, protective coatings for atmospheric exposures and cathodic protection in submerged and buried situations), the relatively high pH of concrete pore water (pH ≈ 13.0-13.6) promotes formation of a protective passive film such that corrosion rate is negligible and decades of relatively low maintenance result.

Corrosion Mechanisms

Disruption of the passive film upon embedded reinforcement and onset of active corrosion can arise in conjunction with either of two causes: carbonation or chloride intrusion (or a combination of these two factors). In the former case (carbonation), atmospheric carbon dioxide (CO_2) reacts with pore water alkali according to the generalized reaction,

$$\mathrm{Ca(OH)_2 + CO_2 \rightarrow CaCO_3 + H_2O}, \qquad (1$$

which consumes reserve alkalinity and eventually reduces pore water pH to the 8-9 range, where steel is no longer passive. For dense, high quality concrete (for example, high cement factor, low water-cement ratio, and presence of a pozzolanic

admixture) carbonation rates are typically on the order of one mm per decade or less; and so loss of passivity from this cause within a normal design life is not generally a concern. On the other hand, carbonation is often a problem for older structures; first, because of age per se and, second, because earlier generation concretes were typically of relatively poor quality (greater permeability) than more modern ones.

Chlorides, on the other hand, can be present in concrete as a consequence of deicing salt usage upon northern roadways or from coastal exposure (or both). While this species (Cl^-) has only a small influence on pore water pH per se, concentrations as low as 0.6 kg/m^3 (1.0 pound per cubic yard (pcy)) on a concrete weight basis have been projected to initiate active corrosion.[1,2] In actuality, it is probably not the concentration of chlorides per se that governs loss of passivity but rather some function of the chloride-to-hydroxide ratio ($[Cl^-]/[OH^-]$), since the latter species (OH^-) is prevalent in pore water and acts as an inhibitor. This has been demonstrated by aqueous solution experiments from which it is apparent that the Cl^- threshold for loss of steel passivity increases with increasing pH.[3,4,5,6,7,8] On this basis, the relative amount of cement in a concrete mix and cement alkalinity are likely to affect the onset of corrosion. Considerable past research effort has focused upon identification of a chloride threshold; however, a unique value for this parameter has remained illusive, presumably because of the role of cement, concrete mix, environmental, electrochemical, and reinforcement (composition and microstructure) variables that are influential.[9,10] Because Cl^- and not carbonation induced loss of passivity is of primary concern for modern bridge structures, subsequent focus in this report is upon this corrosion cause.

Once steel in concrete becomes active, either in conjunction with chlorides achieving a threshold concentration or pore solution pH reduction from carbonation at the embedded steel depth, then the classical anodic iron reaction,

$$Fe \rightarrow Fe^{+2} + 2e^- , \qquad (2$$

and cathodic oxygen reaction,

$$\frac{1}{2}O_2 + H_2O + 2e^- \rightarrow 2OH^-, \quad (3$$

occur at an accelerated rate. Ferrous ions subsequently react to form sequential oxides according to,

$$Fe^{+2} + 2OH^- \rightarrow Fe(OH)_2 \text{ and} \quad (4$$

$$Fe(OH)_2 + O_2 \rightarrow \gamma - FeOOH + H_2O, \quad (5$$

where the latter ferric product (γ–FeOOH) is more protective than the ferrous. Because the ferrous-to-ferric conversion occurs over time and is never complete, passive film disruptions are always ongoing. Also, neither product is protective in the presence of Cl^- or at pH below about 11.5.[11] Despite the normally high alkalinity of concrete, acidification may occur in the vicinity of anodic sites because of oxygen depletion and hydrolysis of ferrous ions according to,

$$Fe^{+2} + 2H_2O \rightarrow Fe(OH)_2 + 2H^+. \quad (6$$

The product H^+ may be reduced and, along with O_2 reduction at more remote cathodic sites, further stimulate the anodic process.

Despite the above, corrosion per se is seldom the cause of failure in reinforced concrete components and structures. This arises because the final corrosion products (either ferric oxide or hydroxide) have a specific volume that is several times greater than that of the reactant steel; and accumulation of these in the concrete pore space adjacent to anodic sites leads to development of tensile hoop stresses about the steel which, in combination with the relatively low tensile strength of concrete (typically 1-2 MPa), ultimately causes cracking and spalling.

Damage of this type has evolved to become a significant concern in the case of coastal bridge sub-structures in Florida. Figure 1 illustrates the deterioration process schematically where chlorides accumulate within the submerged zone from inward sea water migration and in the atmospheric zone as a consequence of capillary flow, splash, and spray. The lack of dissolved oxygen in the submerged zone precludes Reaction 2, and so corrosion is rarely a problem here. However, ready availability of both Cl^- in the splash zone and of O_2 at contiguous, more elevated locations results

in this location (splash zone) being particularly susceptible to corrosion induced damage. Figure 2 shows a photograph of a marine bridge piling that exemplifies corrosion induced concrete spalling in this region.

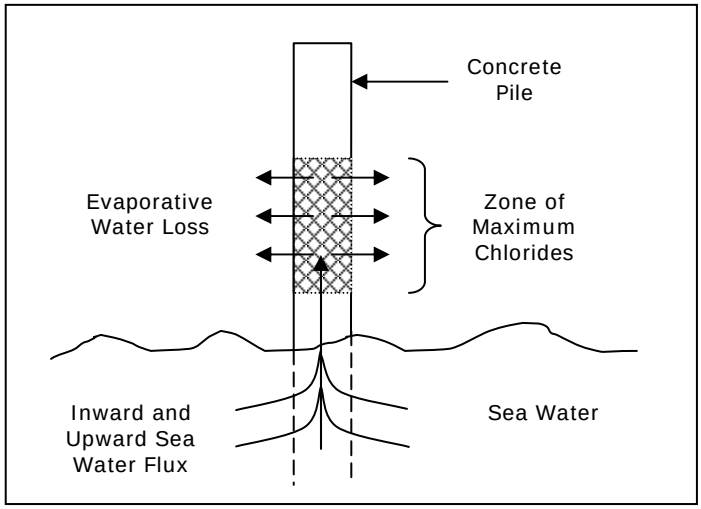

Figure 1: Schematic illustration of sea water migration and Cl^- accumulation within a marine piping.

Figure 2: Photograph of a cracked and spalled marine bridge piling.

Representation of Corrosion Induced Concrete Deterioration

Corrosion induced deterioration of reinforced concrete can be modeled in terms of three component steps: 1) time for corrosion initiation, 2) time, subsequent to corrosion initiation, for corrosion propagation (appearance of a crack on the external concrete surface), and 3) time for one or more surface cracks to develop into spalls that require repair, rehabilitation, or replacement. Figure 3 illustrates these schematically as a plot of cumulative damage versus time showing the above three component times, T_i, T_p, and T_d (periods for initiation, propagation, continued damage (spalling), respectively), as well as the time-to-failure, T_f, or functional service life (modified from Tutti[12]). Of the former three terms, T_i typically occupies the longest period; and so it is upon this parameter that corrosion control measures generally focus. The approach adapted by the Florida Department of Transportation for new bridge construction is to extend the time-to-corrosion initiation by a combination of 1) adequate concrete cover and 2) use of high performance concretes; that is, dense, low water-to-cement ratio concretes with permeability reducing (pozzolanic) or corrosion inhibiting admixtures (or both). Likewise, the methods of Life-Cycle Cost Analysis (LCCA) are employed to evaluate and compare different materials selection and design options. This approach considers both initial cost and the projected life history of maintenance, repair, and rehabilitation

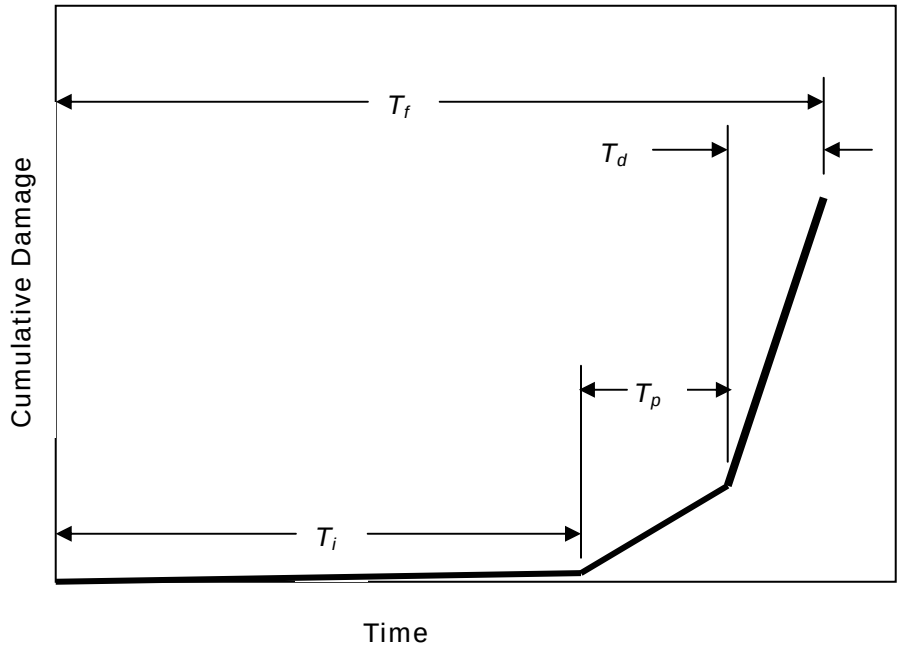

Figure 3: Schematic illustration of the various steps in deterioration of reinforced concrete due to chloride induced corrosion.

expenses that are required until the design life is reached. These are then evaluated in terms of the time value of money, from which Present Worth is determined. Comparisons between different options can then be made on a normalized basis. Figure 4 graphically illustrates an example life-cycle cost scenario.

Analysis of Corrosion Initiation (Time-to-Corrosion)

General

Electrolyte composition is invariably a dominant factor affecting any corrosion process, including that for steel in concrete. As noted above, the predominant corrosion activator in concrete pore water is normally chlorides, whereas hydroxides serve as a passivator. Consequently, T_i for concrete structures is determined by the competing influences of these two species. On the one hand, pore water pH is affected by cement content, cement alkalinity, and exposures that promote carbonation. On the other, chloride concentration, [Cl^-], at the steel depth is determined by 1) composition of this species in the environment, 2) its ingress rate into concrete, and 3) concrete cover over the steel, with onset of active corrosion defined by the Cl^- threshold concentration for passive film breakdown, c_{th}.

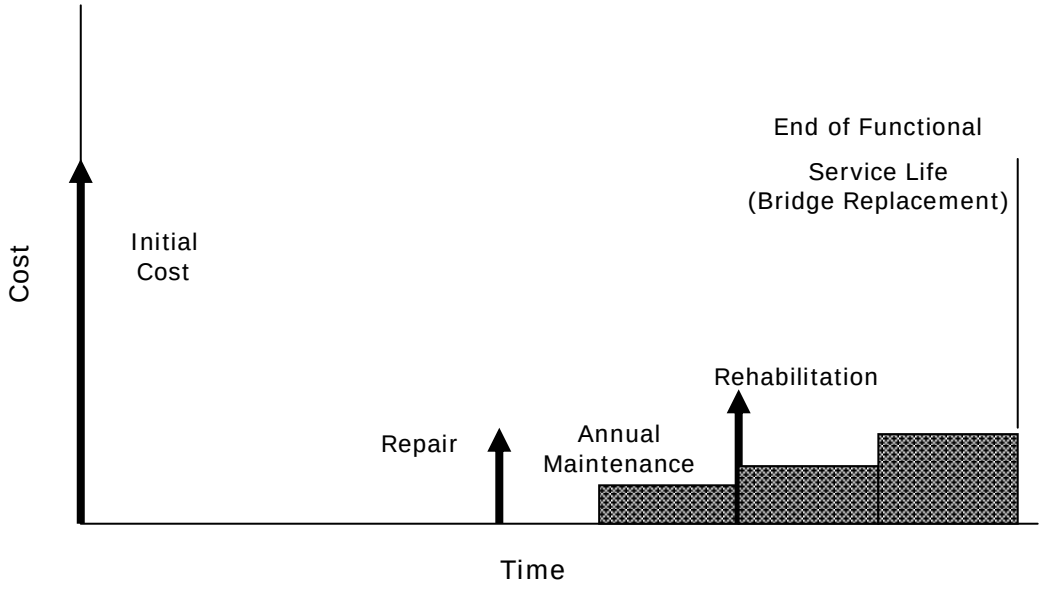

Figure 4: Schematic illustration of life cycle costs.

Pore Water pH

Corrosion experiments intended to simulate steel in concrete have often employed a saturated $Ca(OH)_2$ solution, the pH of which is approximately 12.4. However, with the advent of the pore water expression method[13,14,15] and theoretical considerations, it was recognized that K^+ and Na^+ are the predominant cations; and the solubility and concentration of these is such that a pH in excess of 13 typically occurs.

Limitations associated with pore water expression include, first, prior water saturation of samples is required and, second, the method is more useful for pastes and mortars than concrete since expression yields for the latter, particularly high performance concretes, is low. Consequently, both ex-situ and in-situ leaching methods[16,17] have also been developed, where the former involves exposure of a powder sample to distilled water and the latter placement of a small quantity of water into a drilled cavity in hardened concrete. A limitation in the case of ex-situ leaching is that solid $Ca(OH)_2$ from the concrete becomes dissolved and elevates $[OH^-]$ compared to what otherwise would occur. Also, the dissolved $Ca(OH)_2$, if saturated, buffers the leachate at a pH of about 12.4. These limitations are minimized by the in-situ method because only about 0.4 mL of distilled water is employed; however, water saturation of the specimen is required here also. Recently, a modification of the ex-situ method was proposed whereby a correction is made for the $[OH^-]$ resulting from $Ca(OH)_2$ dissolution;[7,18,19] however, solubles in unreacted cement particles may also become dissolved, thereby elevating the calculated pH compared to what actually exists in the pore water. Consequently, this procedure may be more a measure of inherent alkalinity than of pore water pH.

Chlorides

The mechanism of Cl^- intrusion into concrete invariably involves both capillary suction (sorption) and diffusion; however, for situations where the depth to which the former (capillary suction) occurs is relatively shallow compared to the reinforcement cover, diffusion alone is normally assumed. Analysis of the latter (diffusion) is accomplished in terms of Fick's second law or,

$$\frac{\partial c(x,T)}{\partial t} = \frac{\partial}{\partial t}\left(D \cdot \frac{\partial c(x,T)}{\partial x}\right), \qquad (7$$

where *c(x,T)* is [Cl^-] at depth *x* beneath the exposed surface after exposure time *T* and *D* is the diffusion coefficient. As Equation 7 is written, *D* is assumed to be independent of concentration. The solution in the one-dimensional case is,

$$\frac{c(x,T) - c_o}{c_s - c_o} = 1 - \text{erf}\left(\frac{x}{2\sqrt{D \cdot T}}\right), \qquad (8$$

where

c_o is the initial or background [Cl^-] in the concrete,
c_s is the [Cl^-] on the exposed surface, and
erf is the Gaussian error function.

Assumptions involved in arriving at this solution are, first, c_s and *D* are constant with time and, second, the diffusion is "Fickian;" that is, there are no Cl^- sources or sinks in the concrete. In actuality, c_s may increase with exposure time, although steady-state values in the range 0.3-0.7 (percent of concrete weight) have been projected to result after about six months.[20] Factors that affect c_s include type of exposure, mix design (cement content, in particular), and curing conditions.[21] Also, the diffusion coefficient that is calculated from Equation 8 is an "effective" value, D_{eff}, since it is weighted over the relevant exposure period due to, first, the fact that c_s may vary, second, progressive cement hydration occurs with time, and, lastly, chemical and physical Cl^- binding occur such that the concrete acts as a sink for this species such that some fraction is immobilized.

In the approach represented by Equation 8, *c(x,T)*, c_o, and c_s are measured experimentally (normally by wet chemistry analysis); and D_{eff} is calculated based upon knowledge of reinforcement cover and exposure time. Experimental scatter and error may be minimized by measuring *c(x,T)* at multiple depths and employing a curve-fitting algorithm to calculate D_{eff}. Also, if D_{eff} is known from one sampling set, then c_{th} can be determined by measuring *c(x,T)* at the reinforcement depth (c_{rd}) at the time and location of corrosion initiation and solving Equation 8 recognizing that for this situation, $c_{rd} \approx c_{th}$. In any case, the parameters that affect Cl^- intrusion rate are c_s, and D_{eff}, both of which depend upon exposure conditions such as temperature, relative humidity, and time-of-wetness and material variables such as composition and microstructure.

A factor that is not normally considered in time-to-corrosion evaluations is that c_s, x, c_{th}, and D_{eff} are statistically distributed parameters. Consequently, T_i also conforms to some distribution. This is important because decisions regarding repairs and rehabilitations are often based upon damage having occurred over some percentage of the structure. Alternatively, loss of a single critical, non-redundant structural element (substructure bridge pier, for example) causes failure.

Values for c_{th} in the range 0.60-0.75 kg/m^3 (1.0-1.3 pcy) have historically been reported and referenced for concrete structures in North America.[1,2] However, this parameter, c_{th}, is now recognized as depending upon multiple factors, including 1) concrete mix design (w/c, cement content), 2) exposure conditions, and 3) reinforcing steel surface condition,[8] as noted above. From literature data, Glass and Buenfeld[9] reported values in the range 0.17-2.5 (total Cl^- on a cement w/o basis) or, alternatively, 0.66-9.71 kg/m^3 (concrete weight basis assuming 400 kg/m^3 cement content). Thus, the topic of what constitutes a correct value for c_{th} and upon what factors it depends continues to be of interest from both a research and technological perspective.

The approach of employing pozzolanic and corrosion inhibiting admixtures that has been adapted by the FDOT for enhancing concrete durability, as noted above, can be related to and interpreted in terms of Equation 8. In this regard, the most prevalent corrosion inhibitor ($Ca(NO_2)_2$), in effect, increases c_{th}, whereas pozzolans (fly ash, silica fume, and blast furnace slag) reduce D_{eff}. Surface [Cl^-] may also be affected by pozzolans.

It is generally thought that c_{th} increases with increasing cement alkalinity,[10] although it is but recently that a systematic investigation was performed that quantitatively confirmed this.[22,23] For some geographical locations, concerns regarding alkali-silica reaction (ASR), whereby aggregates swell from chemical reaction with alkaline pore water, preclude utilizing high alkalinity cements, since ASR should occur at a greater rate the higher the pore water alkalinity. The native Florida limestones that serve as coarse aggregate for concrete bridge construction in most of the State are not considered susceptible to ASR, however. Consequently, if it can be demonstrated that c_{th} for high alkalinity cements exceeds that for normal ones, then use of these cements should yield concrete structures with enhanced

resistance to corrosion induced deterioration but with no additional cost or construction complexity.

PROJECT BACKGROUND

In an earlier FDOT sponsored project (WPI 0510716), 160 reinforced concrete slab type specimens of various mix designs, including control specimens (no admixtures) and specimens with various amounts of admixed fly ash or silica fume and with and without a corrosion inhibitor (calcium nitrite), were cyclically ponded with natural sea water.[18] Concrete cover was either 19 or 32 mm (0.75 or 1.25 inches). In all cases, a water-to cementiteous ratio of 0.37, which is consistent with the FDOT specification for Class V concrete, was employed. Figure 5 shows a schematic illustration of this specimen type, while Figure 6 shows a photograph of an individual specimen under test. A photograph of the overall exposures is seen in Figure 7. To-date, some nine years after ponding commenced, reinforcement potentials remain relatively positive and macro-cell currents negligible, which is indicative of passivity. Consequently, it has not been possible to determine the admixture type and mix design dependence of the chloride threshold. Quantification

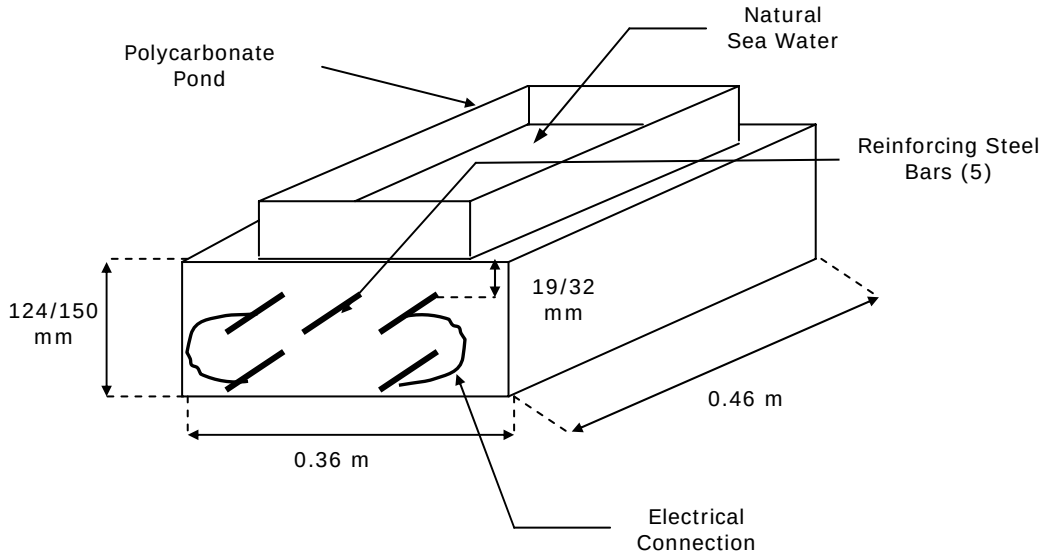

Figure 5: Schematic illustration of concrete slab specimen from Project WPI 0510716.

Figure 6: Photograph of an individual concrete slab specimen from the previous admixture project.

Figure 7: Photograph of specimens from the admixture project under test.

of this parameter (chloride threshold for corrosion initiation) is critical to 1) affecting accurate projections of when corrosion initiation will occur for actual structures (design concrete covers of 75 mm (3 inches) for prestressed and 100 mm (4 inches) for cast-in-place) and 2) making informed decisions with regard to repair and rehabilitation planning. Cores were taken from blank specimens after 3.7 years exposure, the Cl^- profiles measured, and D_{eff} calculated. Table 1 lists the results

from this and indicates D_{eff} values for admixed specimens that approach being an order of magnitude less than for the control.

Table 1: Diffusion coefficients for the different concrete mix designs.

Mix Design Designation	Fly Ash, percent	Silica Fume, percent	Calcium Nitrite, l/m^3 (gal/y^3)	Diffusion Coef., m^2/s (in^2/y)
AO	0	0	0	$3.18 \cdot 10^{-12}$ (0.16)
FA1	20	0	0	$7.44 \cdot 10^{-13}$ (0.04)
FA2	35	0	0	$6.77 \cdot 10^{-13}$ (0.03)
FA3	50	0	0	$4.96 \cdot 10^{-13}$ (0.02)
FA4	35	0	19.8 (4.0)	$6.68 \cdot 10^{-13}$ (0.03)
SF1	0	6	0	$1.72 \cdot 10^{-12}$ (0.08)
SF2	0	15	0	$2.10 \cdot 10^{-13}$ (0.10)
SF3	0	27	0	$9.26 \cdot 10^{-13}$ (0.05)
SF4	0	15	9.9 (2.0)	$9.30 \cdot 10^{-13}$ (0.05)

In a follow-on project (BD776), which commenced in 1998, a series of 91 G109[24] specimens began a cyclic one week wet – one week dry ponding exposure with 15 weight percent (w/o) NaCl. The objective of these exposures was to evaluate an alternative or complementary approach to pozzolonic and corrosion inhibiting admixtures for affecting reinforcement corrosion resistance based upon elevated cement alkalinity. Thus, as noted above, chlorides are a corrosion activator and hydroxides, as promoted by cement alkalinity and a corresponding elevation in pore water pH, serve as an inhibitor. On this basis, several investigators[18,25,26,27,28,29] have reasoned that corrosion initiation should not necessarily be a function of chloride concentration per se but of the ratio of chlorides to hydroxides $[Cl^-]/[OH^-]$. Consequently, use of high alkalinity cements for the purpose of affecting a relatively high pore water pH appears to be an option in Florida since, unlike some areas of the United States, the local limestone aggregates are relatively resistant to reaction with alkali. The fundamental objective of these projects was to investigate the extent to which high alkalinity cements could extent T_i for Florida concrete bridge substructures.

Figure 8 provides a schematic drawing of the G109 type specimen, and Figure 9 shows a photograph of two specimens under test. Table 2 presents the specimen matrix for this prior program and shows that cements of three Equivalent Alkalinities (Na_2O_e), 0.972, 0.519, and 0.355, as calculated from the expression,

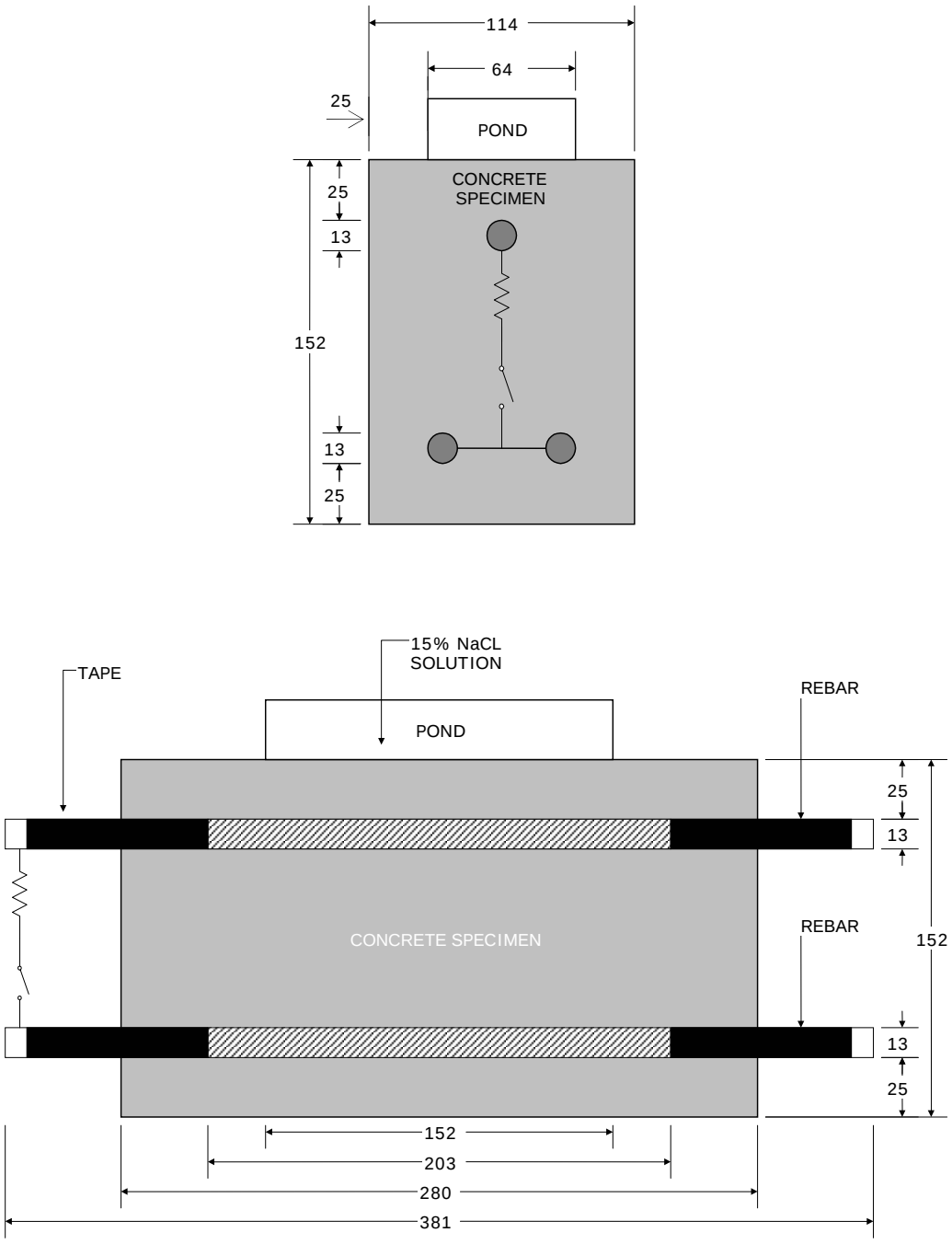

Figure 8: Geometry of the G109 type specimens.

$$Na_2O_e = w/oNa_2O + 0.658 \cdot w/oK_2O, \qquad (9$$

where w/o is weight percent of the indicated compound, were employed. These were designated as “high” or HA, “normal” or NA, and “low” or LA, respectively. The

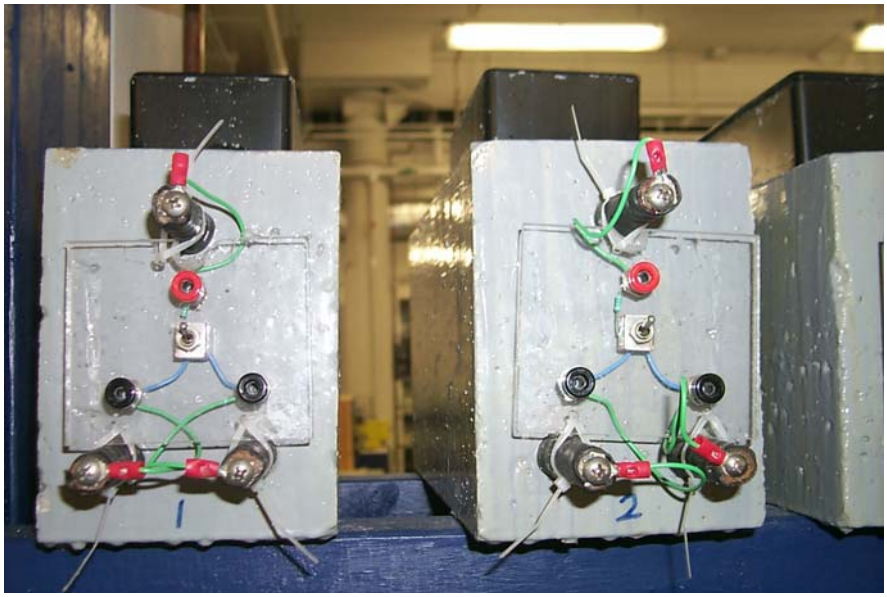

Figure 9: Photograph of two G109 specimens undergoing cyclic salt water ponding exposure.

Table 2: Specimen matrix for investigation of the effect of cement alkalinity upon the onset of embedded steel corrosion.

Specimen No.	Reinforcement	Cement Alk.	w/c		Specimen No.	Reinforcement	Cement Alk.	w/c
01-04, 85-88*	Yes	High	0.37		43-46	Yes	Low	0.37
05-07, 89-91*	No				47-49	No		
08-11	Yes	High	0.41		50-53	Yes	Low	0.41
12-14	No				54-56	No		
15-18	Yes	High	0.50		57-60	Yes	Low	0.50
19-21	No				61-63	No		
22-25	Yes	Normal	0.37		64-67	Yes	HAG**	0.37
26-28	No				68-70	No		
29-32	Yes	Normal	0.41		71-74	Yes	NAF***	0.41
33-35	No				75-77	No		
36-39	Yes	Normal	0.50		78-81	Yes	NAF***	0.50
40-42	No				82-84	No		

* Ponded with natural sea water. All others with 15w/0 NaCl.
** High alkalinity grout (no coarse aggregate).
*** Normal alkalinity cement with 20w/o fly ash replacement.

Low and Normal Alkalinity cements are typical of what is presently employed in Florida bridge construction, whereas the High is beyond the normally specified limit by nearly 0.4 units. Table 2 indicates that additional variables in the specimen

matrix were 1) water-cementiteous ratio, 2) presence versus absence of fly ash, and 3) natural sea water versus 15 percent NaCl solution ponding.

As was the case for the pozzolanic admixtured concrete slabs,[18] unexpectedly long times-to-corrosion were encountered for these specimens as well, although at the official completion of the project (December 31, 2002) 28 of the 52 reinforced G109 specimen had indicated active corrosion. Specific findings from this project included the following:

1. Time-to-corrosion for "identical" specimens of each mix design varied, often over a relatively wide range. This resulted because T_i is statistically distributed and is affected by a number of factors, each of which is also distributed. Time-to-corrosion was least for concrete specimens with the NA cement, intermediate for the LA, and highest for HA. Figure 10 provides a cumulative distribution function plot of T_i based upon Weibull analysis. It was concluded that improved corrosion resistance can be realized using cements of the HA type. The increase in T_i for

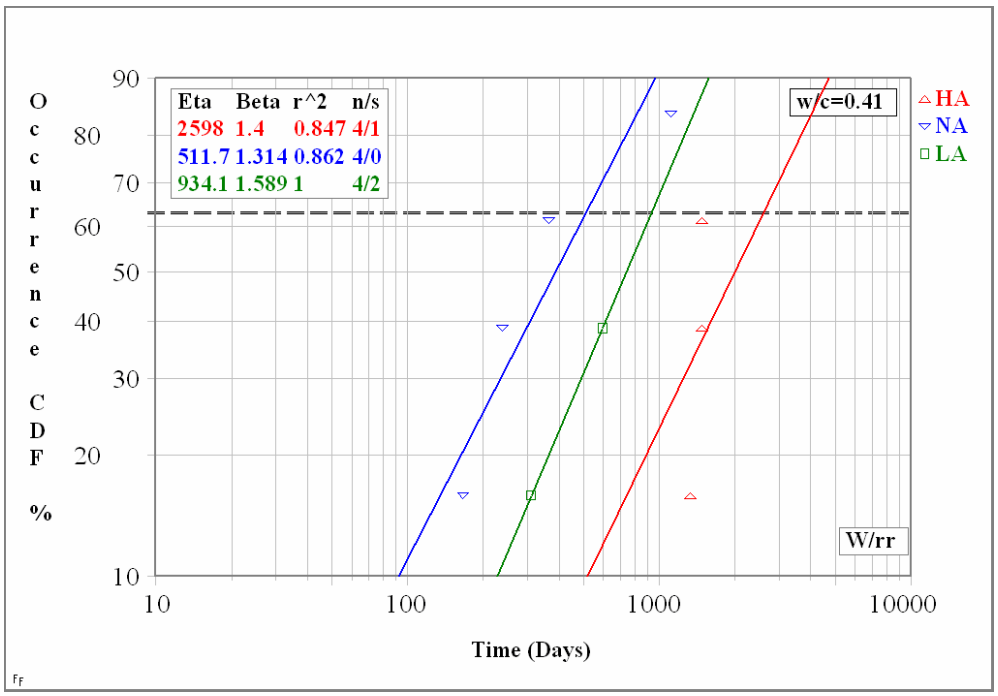

Figure 10: Two-parameter Weibull distribution of the T_i data for specimens with water-cement ratio 0.41. Values for eta (mean), shape parameter (beta (β was forced at 1.40 in the HA specimen case)), and the number of failures (n) and suspensions (s) are indicated.

specimens with the HA cement compared to the NA ones was by approximately a factor of three for water-cement ratio 0.37 and by a factor of ten for water-cement ratio 0.41. That T_i did not increase in direct proportion to increasing cement alkalinity was thought to have resulted from relatively high Cl^- binding at lower pore water pH.

2. Pore water pH was in the range 13.05-13.20 for the LA mix concrete, 13.19-13.36 for the NA, and 13.53-13.65 for the HA. This resulted from OH^- concentration for the HA cement concrete being about a factor of two greater than for the NA. Figure 11 summarizes these results and indicates that the pH-cement alkalinity trend for the present concretes was slightly above the lower bound of data in the literature.[30,31,32,33,34,35,36,37,38,39]

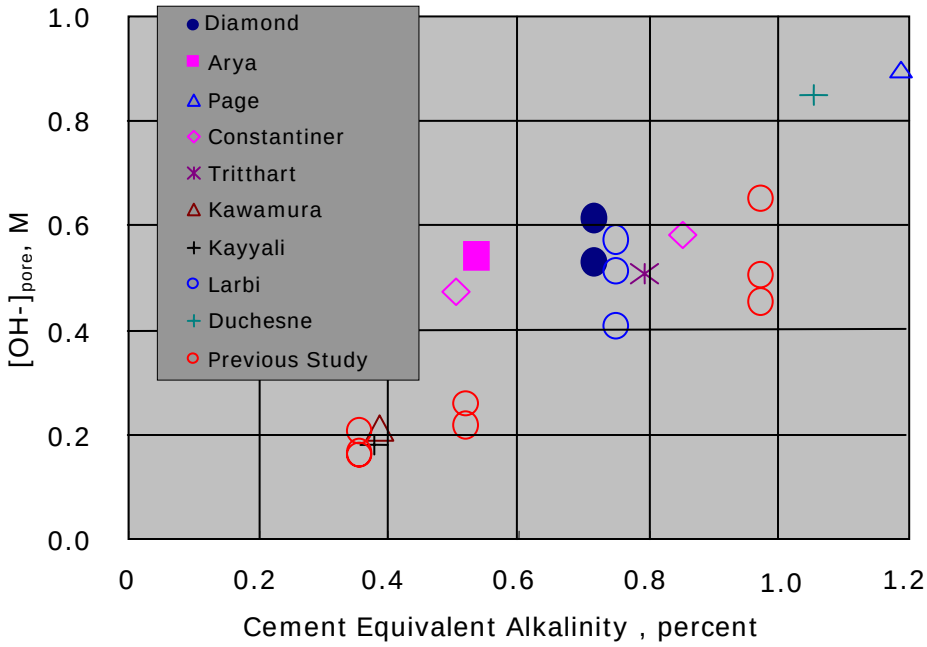

Figure 11: Relationship between pore water [OH^-] and cement equivalent alkalinity as determined by the ex-situ method and by past research.

3. The threshold chloride concentration to cause passive film breakdown and active corrosion, c_{th}, increased with increasing T_i. Consequently, the HA specimens exhibited the highest c_{th} although all data conformed to a common trend. Local chloride concentrations in the concrete measured from powder drillings taken along the top side of the upper rebar trace once specimens were opened varied

from 7.84 to 27.64 kg/m^3 (concrete w/o basis) at the site of active corrosion and from 4.31 to 23.52 kg/m^3 at locations where the steel was passive. This difference presumably resulted from electromigration of Cl^- to active sites subsequent to corrosion initiation. The latter range (4.31 to 23.52 kg/m^3) was considered to represent c_{th}, since Cl^- electromigration and rapid accumulation of this species subsequent to corrosion initiation should not have occurred here; however, it exceeds what is typically assumed to initiate reinforcement corrosion in North American bridge deck concretes (0.60-0.75 kg/m^3 (1.0-1.3 pcy)) by a factor of 6-39. On the other hand, the general literature reports the range for c_{th} as 0.66-9.71 kg/m^3 which, while overlapping, is still less than was measured in this study. Figure 12 illustrates these data.

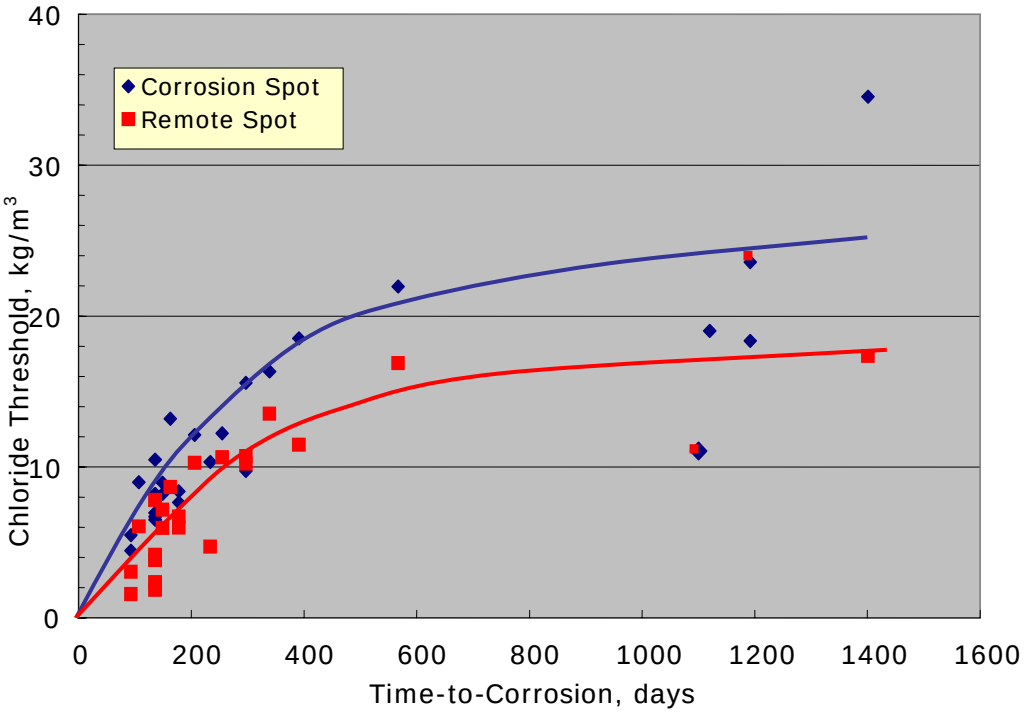

Figure 12: Plot of Time-to-Corrosion as a function of [Cl^-] for specimens that had become active.

4. The effective diffusion coefficient, D_{eff}, increased with increasing water-cement ratio and was about 40 percent lower for concrete prepared with the HA cement compared to the NA and LA ones. The present D_{eff} values are at the upper bound or exceed those reported in the literature. Results from short-term exposures

indicated that sorption was a significant contributor to Cl^- uptake, and this apparently inflated the D_{eff} determinations. This role of sorption also brings into question the appropriateness of Fick's second law for analyzing Cl^- diffusivity in specimens of this type where concrete is relatively porous (high w/c) and cover relatively low.

5. In situations where observations were made, corrosion was found to have initiated at a void in the concrete that impinged upon the reinforcement. A concentration cell whereby the contiguous concrete coated and bare steel served as cathode and anode, respectively, was considered to have been responsible. The size and density distribution of these voids may have contributed to or been responsible for the finding that T_i was a distributed parameter.

PROJECT OBJECTIVE

The purpose of this research was to better understand the dependence of the chloride threshold upon the mix design variables listed above and possible other factors including 1) differences in temperature and relative humidity and 2) reinforcement surface condition. The study involved continued monitoring and analysis of existing specimens and new experiments that extended the existing tests to include the factors listed above. Also, some specimens were larger than the standard G109 in order to define and quantify how the onset of corrosion might be affected by statistical aspects of microstructural features associated with the reinforcement-concrete interface.

EXPERIMENTAL PROCEDURE

Time-to-Corrosion and Chloride Threshold Experiments

Three types of specimens were employed in this research, as listed below:

1. Standard G109,[24] both a new set and ones from the previous study.

2. Oversized G109 type specimens.

3. Simulated piling specimens (FDOT developed “tombstone”).

A schematic illustration of the standard G109 Type 1 specimen was provided in Figure 8, and Figure 9 shows a photograph of two specimens under test. The oversized G109 specimens were geometric 2X, 4X, and 8X multiples of the standard G109 cast as a single unit. A photograph of these is shown in Figure 13. Likewise, Figures 14 and 15 show a drawing and photograph, respectively, of the Type 3 specimen. The standard G109 and tombstone specimens (Types 1 and 3 above)

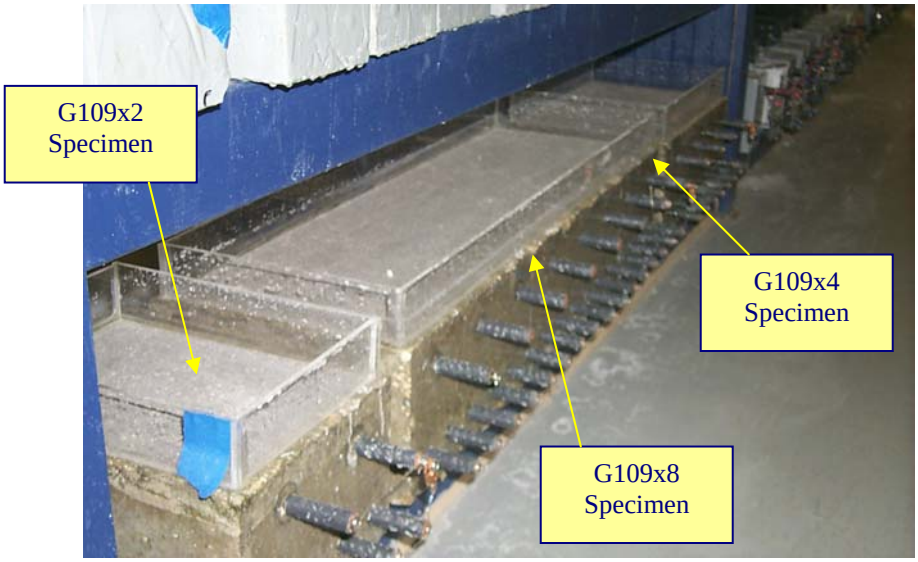

Figure 13: Photograph of oversized G109 specimens.

were based upon mix designs with w/c = 0.50 and 0.37 and cements of two alkalinities. Table 3 gives the composition for these cements and shows that the Na_2O_e values were 0.317 and 1.078 percent. By comparison, Na_2O_e values in the earlier program (Contract No. BC 776, see above) were 0.355, 0.519, and 0.972 and were designated LA, NA, and HA, respectively. On this basis, the low and high Na_2O_e cements in the present study were designated LA and HA and were considered comparable to their previous study counterparts. Mix designs based upon the lower w/c (0.37) and low and normal alkalinity cements are typical of current FDOT practice, disregarding inclusion of a pozzolonic and a corrosion inhibiting admixture. Research results to-date indicate that high Na_2O_e elevates c_{th}.[22,23] The higher w/c mix was included to best insure that at least some data would be acquired in a

timely manner. These LA and HA G109 specimens were similar to those from the prior

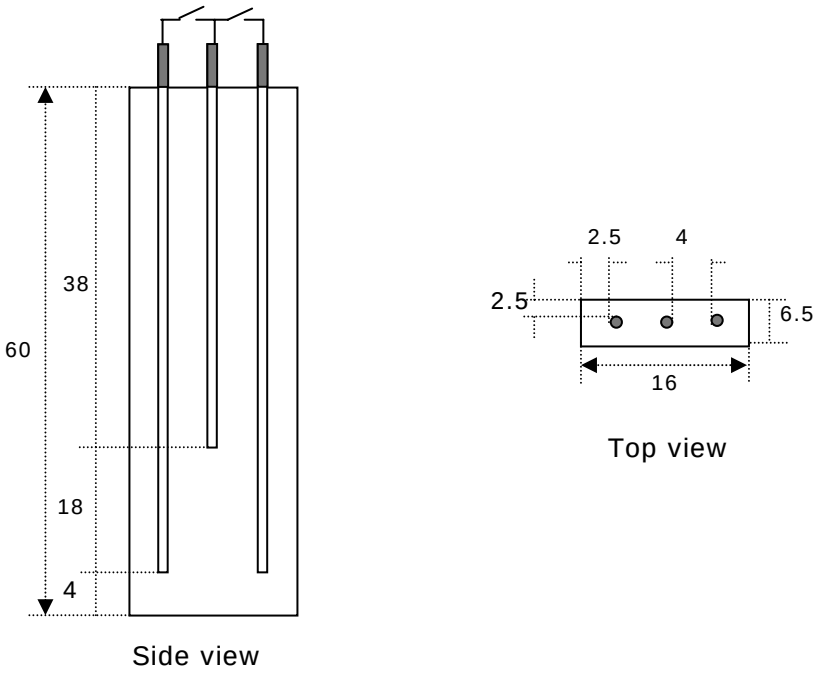

Figure 14: Schematic illustration of the Type 3 specimen.

Figure 15: Photograph of a Type 3 specimen upon removal from exposure tank.

project that have been under test for over five years and which have exhibited exceptionally high c_{th} (see Figure 12). The new specimens were intended to extend

Table 3: Compositional analysis results for the two cements.

	Value, percent	
Component	Low	High
SiO_2	19.83	20.40
Al_2O_3	4.94	5.33
Fe_2O_3	4.59	2.70
CaO	64.84	62.78
MgO	0.85	2.61
SO_3	2.78	4.02
Na_2O	0.126	0.274
K_2O	0.29	1.22
TiO_2	0.23	0.28
P_2O_5	0.082	0.165
Mn_2O_3	0.060	0.072
SrO	0.079	0.098
F	0.049	0.052
Cr_2O_3	0.002	0.002
C3A	5.322	9.539
C3S	5.623	49.422
C2S	7.683	21.493
Equivalent Alkalinity	0.317	1.078
SS (C4AF+C2F)	18.173	15.784
C4AF	13.956	8.225
S	1.113	1.606

the database obtained with past ones and to provide additional opportunities for understanding the mix design – chloride threshold – time-to-corrosion relationship. Once specimens became active, they were broken open at the horizontal plane of the upper rebar, the steel examined, and powder samples taken by drilling the concrete along the top of the bar trace. These samples were analyzed for chlorides using the FDOT acid soluble titration method, FM 5-516.[40]

The oversized G109 specimens (item 2 above) were of the higher w/c (0.50) and LA cement only. The simulated piling specimens (Type 3) provided a situation of greater wetness and are intended to have more direct applicability to Florida marine bridge substructures. All specimens were fabricated by the FDOT Corrosion Laboratory in Gainesville.

The first generation G109s specimens began cyclic ponding with a 15 weight percent (w/o) NaCl solution in July, 1998, such that the ones that have not initiated corrosion and that remain have now been under test for over 2,000 days. Exposure of the second generation Type 1 and 2 specimens has been for as long as 300 days. The Type 1 tests were conducted under five exposure conditions, as listed in Table 4. The differences reflected here were intended to provide information regarding the influence of relative humidity (RH) and temperature, as both static (conditions C1-C3) and time variable (conditions C4 and CO) parameters, upon c_{th}. Figure 16 schematically illustrates the test chamber for temperature/RH control. The Type 2 specimens were exposed under the C1 condition (ambient laboratory) only. Type 3 specimens, on the other hand, have been exposed for as long as 196 days. Testing

Table 4: Listing of exposure conditions.

Designation	Condition
C1	Normal laboratory RH (~50-60 %) and temperature (~23^{o}C).
C2	RH constant at 80% and normal laboratory temperature.
C3	RH constant at 80% and temperature 40^{o}C.
C4	Weekly cycle between 20 and 40^{o}C with RH ~ 80%.
CO	Outdoors.

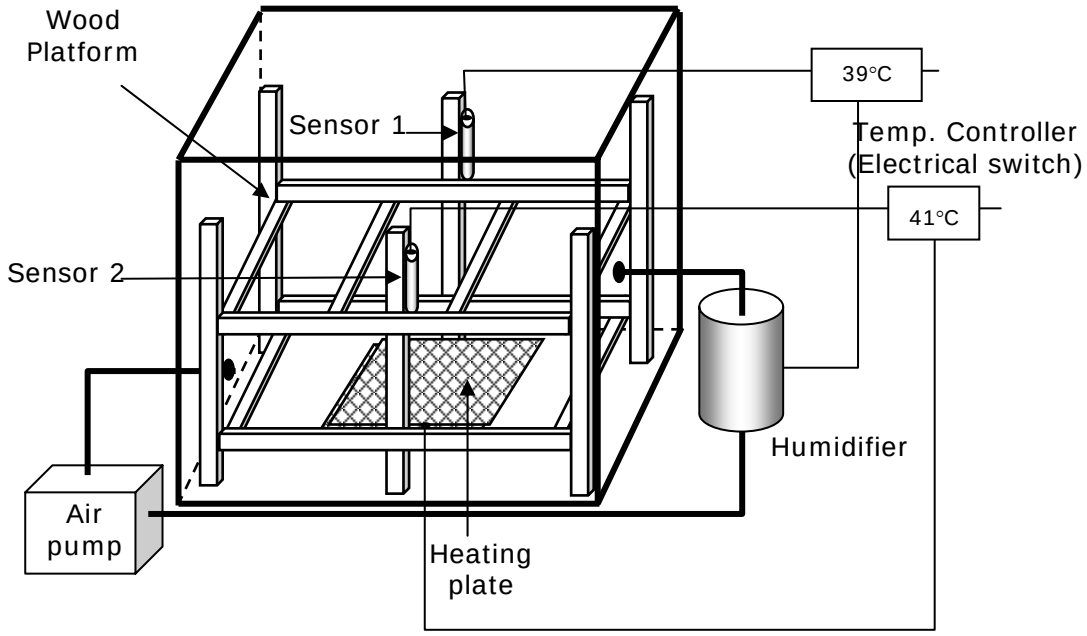

Figure 16: Schematic illustration of a Type 1 specimen temperature/RH control exposure chamber.

of the Type 1 and 2 specimens involved repetitive one week wet – one week dry cyclic ponding with 15 w/o NaCl, which is the same as for the earlier generation specimen set. Type 3 specimens were continuously exposed partially submerged in the same solution. In some cases, water level (WL) was constant with specimens positioned vertically such that the bottom 15 cm was submerged, whereas for others WL was cycled between 10 and 20 cm at 12 hour intervals. Figure 17 shows a schematic illustration of the cyclic WL test setup, and Figure 18 is a photograph of the Type 3 specimens under test.

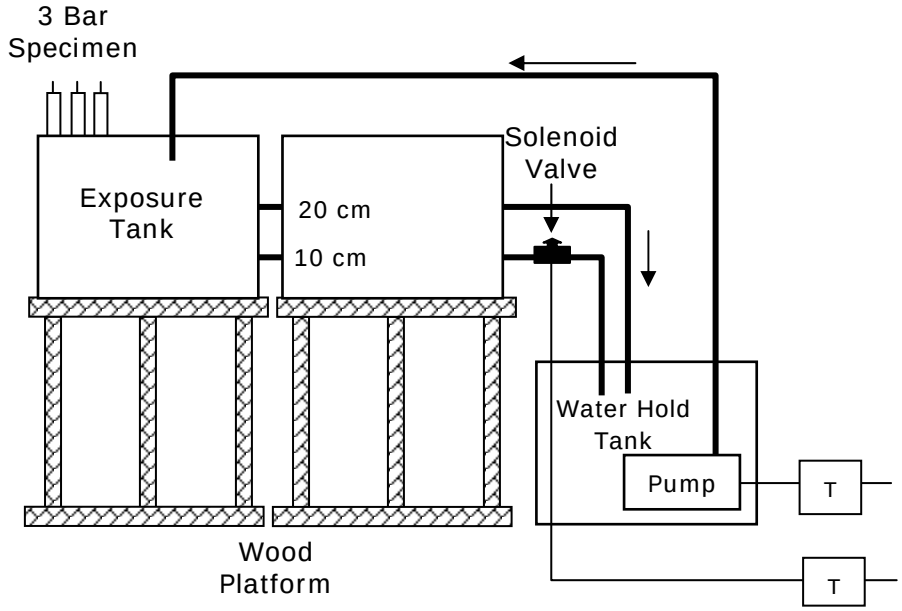

Figure 17: Schematic illustration of the Type 3 specimen test setup.

Reinforcement surface condition was either wire-brushed (P) or as-received (AR), where the latter exhibited mill scale with some atmospheric rusting. Table 5 summarizes the test matrix. A minimum of four Type 1 and three Type 3 specimens were tested for each condition. Monitoring and data acquisition for the Type 1 and 2 specimens included potential and macro-cell current and for the simulated piling specimens (Type 3) potential alone.

Chloride Diffusion Coefficient Determinations

A set of experiments was also performed to better understand the effect of RH on the effective diffusion coefficient (D_{eff}). This involved exposure of cylindrical, non-reinforced concrete specimens in constant RH chambers at ambient laboratory

Figure 18: Photograph of Type 3 specimens under test.

Table 5: Project test matrix.

		Specimen Type									
		1						2	3		
Spec. Type	Spec. Mix Design*	Indoor					CO		Indoor		
		C1		C2	C3	C4		C1	Const. WL	Cyclic WL**	
		AR	P							AR	P
1	LA0.50	*	*	*	*	*	*	-	-	-	-
	LA0.37	*	*	*	*	*	*	-	-	-	-
	HA0.50	*	*	-	-	-	-	-	-	-	-
	HA0.37	*	*	-	-	-	-	-	-	-	-
2	LA0.50	-	-	-	-	-	-	*			
3	LA0.50	-	-	-	-	-	-		*	*	*
	LA0.37	-	-	-	-	-	-		*	*	*
	HA0.50	-	-	-	-	-	-			*	*
	HA0.37	-	-	-	-	-	-			*	*

* Letters indicate the cement alkalinity (LA versus HA) and the numbers w/c.

temperature with the top specimen surface being sprayed on alternate days, subsequent to equilibration, with a 15 w/o NaCl solution. The mix design was as listed in Table 6. Target RHs were 35, 55, 75, and 95 percent. The former two values were achieved by flowing an appropriate mixture of RH 20 and 75 air through the respective chambers. Relative humidities of 75 and 95 were achieved by placement of a saturated NaCl–distilled water solution and distilled water,

respectively, in the chamber bottom and elevating the specimens above this. Figure 19 illustrates the test arrangement schematically. Three specimens were exposed in each of the four chambers, where one of these was used for Cl^- profiling after three months exposure and a second after six months. A RH probe was mounted in a sealed hole drilled in the third specimen so that RH within the concrete itself could be monitored. Figure 20 is a schematic illustration of the two specimen types; and Figure 21 shows a photograph of the overall test arrangement including RH probes mounted in concrete specimens and meters. A fifth specimen set was cycled between the 35 and 95 RH chambers on alternate days.

Table 6: Concrete mix design for the constant RH experiments.

Material	Amount, kg/m^3
Cement	400
Fine Aggregate (Silica Sand)	794
Coarse Aggregate (Florida Limestone, #89)	859
Water	180
Water-Cement Ratio	0.45

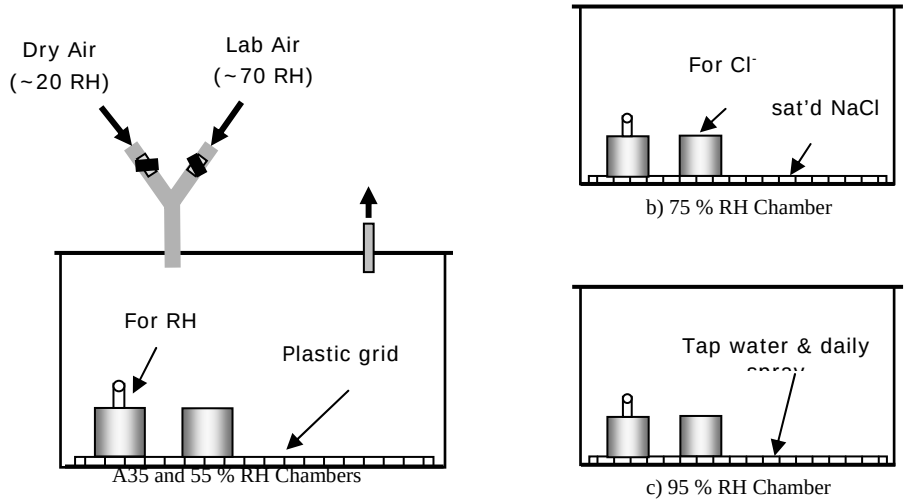

Figure 19: Schematic illustration of the constant RH chambers.

A second set of the same concrete specimens as for the constant RH exposures was employed for D_{eff} determinations as a function of temperature. The exposures involved four temperatures: 0°C, ambient (~20°C), 30°C and 40°C, where the first was affected by placement in a freezer, the second in ambient laboratory air, and the latter two using the same type of controlled temperature chamber as in Figure 16.

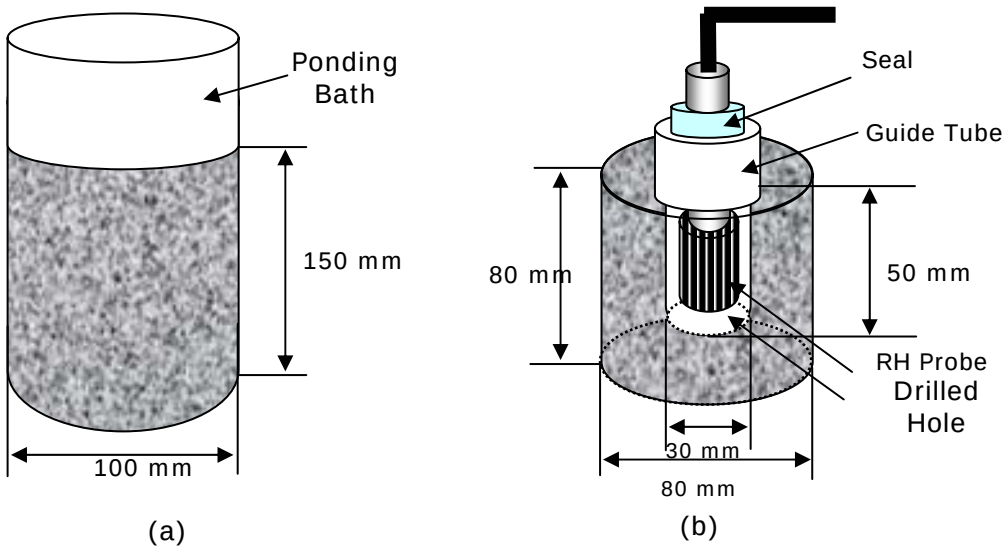

Figure 20: Schematic illustration of concrete specimens for (a) chloride profile determination and (b) internal RH measurement.

Figure 21: Photograph of constant RH chambers with specimens, embedded RH probes(2), and meters(2).

Duplicate specimens were employed for 0, 30, and 40°C and 12 specimens for 20°C. Specimens were the same as for the constant RH tests but with continuous 15 w/o NaCl ponding (RH was not controlled because the ponding was continuous and not cyclic). An additional specimen pair was cycled between 20 and 40°C on alternate days. Chloride profiles were determined for one specimen of each of the pairs after three months exposure and for the second after six months. In all cases, chloride

analyses were made by, first, slicing the cylinders at appropriate intervals, grinding the slices to powder, and, lastly, analyzing also using the FDOT method.[40] The Cl^- profile data were fitted to a least-squares algorithm for Equation 8, from which D_{eff} was calculated.

RESULTS AND DISCUSSION

Time-to-Corrosion

Specimen Type 1

Figures 22-26 report environmental conditions for the initial period of the exposure for conditions C1-C4 and for a period near the end of the condition CO (outdoors) exposure, respectively. These indicate that the target values for both RH and temperature were approximately achieved.

In the previous study,[22,23] T_i was defined as the time at which potential equaled or became more negative than -0.280 V_{SCE} and macro-cell current equaled or exceeded 10 μA. For specimens that became active relatively early in the program (T_i less than about 300 days) these two criteria were reached concurrently; however, for T_i greater than about 600 days this was not always so, in which case the onset of corrosion was defined according to the criterion that was achieved first. For the present specimens, corrosion activity commenced at a reduced exposure time compared to the previous ones (see Figure 10); and the potential and current criteria

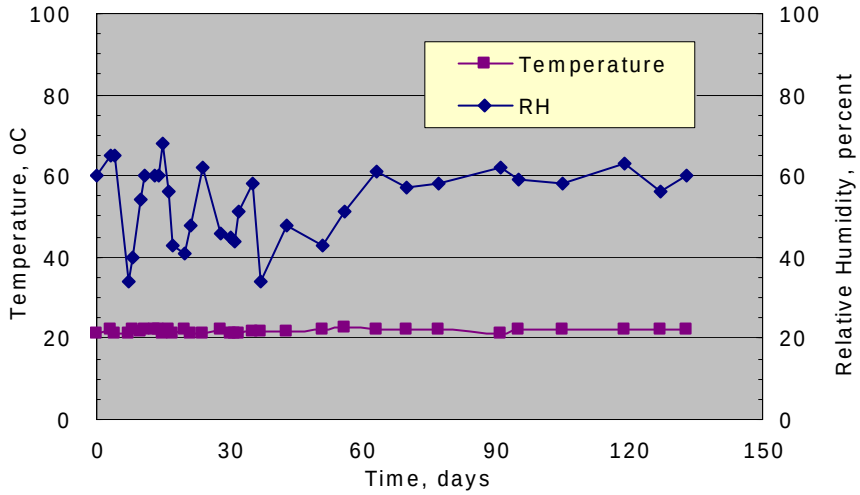

Figure 22: Environment parameters for exposure condition C1.

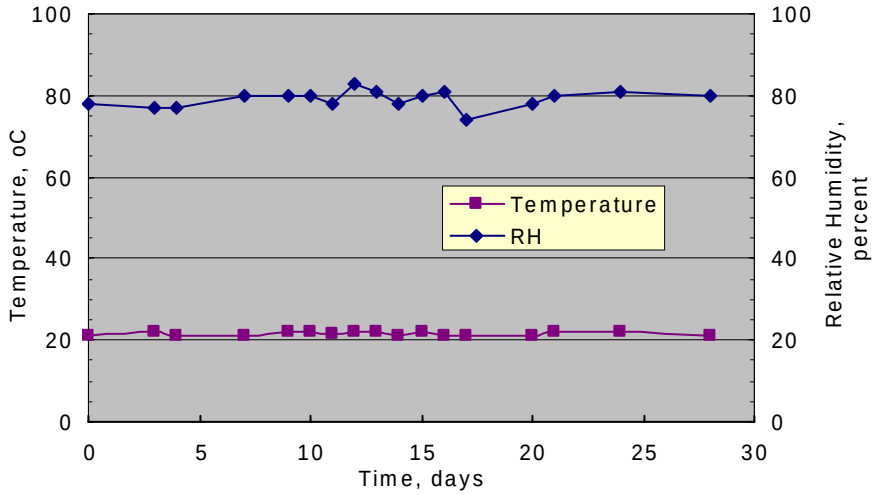

Figure 23: Environment parameters for exposure condition C2.

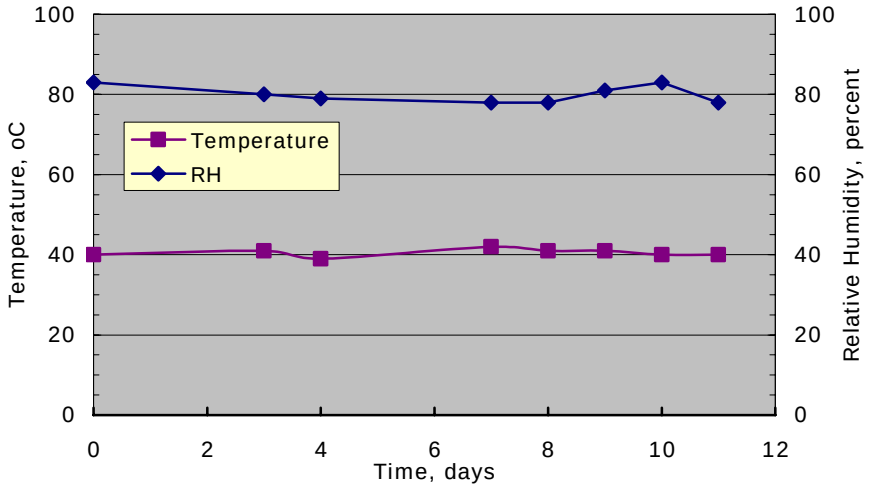

Figure 24: Environment parameters for exposure condition C3.

was so brief, no temperature cycling occurred; and so this exposure was the same as for C3.

Table 7 provides a listing of all C1 exposure specimens along with T_i, as defined by both criteria, and the exposure time at which autopsy occurred (T_A). Likewise, Table 8 does the same for the C2, C3, and C0 exposures.[i] This reveals cases of criterion concurrence (Specimen 13) and difference (Specimens 7 and 12, for

[i] In Tables 7 and 8 and in subsequent discussion, T_i as defined by the potential criterion is designated T_p and by the macrocell current criterion, T_l.

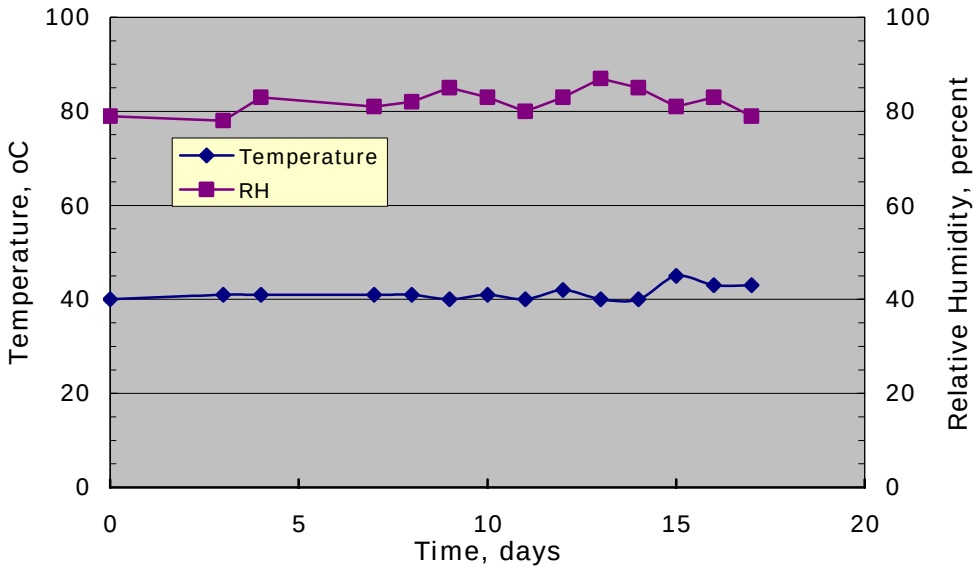

Figure 25: Environment parameters for exposure condition C4.

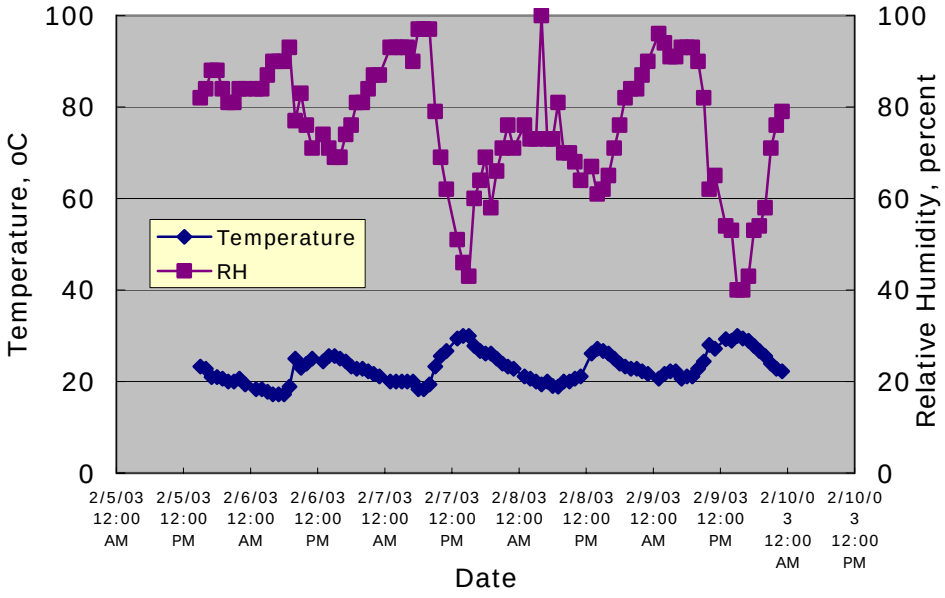

Figure 26: Environment parameters for Ft. Lauderdale area in the general time of the outdoor exposures.

example) with no trend being apparent. Figures 27 and 28 show potential and macro-cell data versus time for Specimens 5-8 and 23-26, respectively, as examples of the different trends. However, the potential shift to more negative values invariably coincided with a macrocell current increase, suggesting that both

Table 7: T_i data for Type 1 specimens exposed under the C1 condition.

Specimen No.	Mix Design	T_P	T_I	T_A
1	LA0.50	24	21	28
2		27	20	28
3		20	16	21
4		25	21	32
5		14	11	14
6		58*	35	58
7		30	20	32
8		18*	13	14
9		24	20	28
10		28	20	28
11	LA0.50-P	34	22	35
12		35	17	35
13		20	20	21
14		32	32	35
15	LA0.37	>393	267	>393
16		>393	>393	>393
17		>393	267	>393
18		>393	112	>393
19	LA0.37-P	112	84	141
20		>393	>393	>393
21		>393	>393	>393
22		>393	277	>393
23	HA0.50	194	141	197
24		112	95	112
25		141	119	155
26		127	56	141
27	HA0.50-P	197	197	197
28		105	83	112
29		311	245	311
30		190	141	197
31	HA0.37	>393	>393	>393
32		>393	>393	>393
33		>393	>393	>393
34		>393	>393	>393
35	HA0.37-P	>393	>393	>393
36		>393	>393	>393
37		>393	>393	>393
38		>393	>393	>393

P: Wire brush surface preparation. Other specimens as-received.
* Value estimated by extrapolation.

Table 8: T_i data for Type 1 specimens exposed under the C2, C3, and C0 conditions.

Specimen No.	Mix Design	Exposure	T_p	T_I	T_A
39	LA0.50	C2	11	10	11
40			21	12	21
41			10	8	9
42			23	18	28
43		C3	11	9	11
44			9	7	9
45			7	4	8
46			10	7	9
47			17	15	17
48			17	14	17
49			14	8	9
50			14	10	11
51		CO	30	18	28
52			13	11	12
53			16	12	14
54			14	10	14

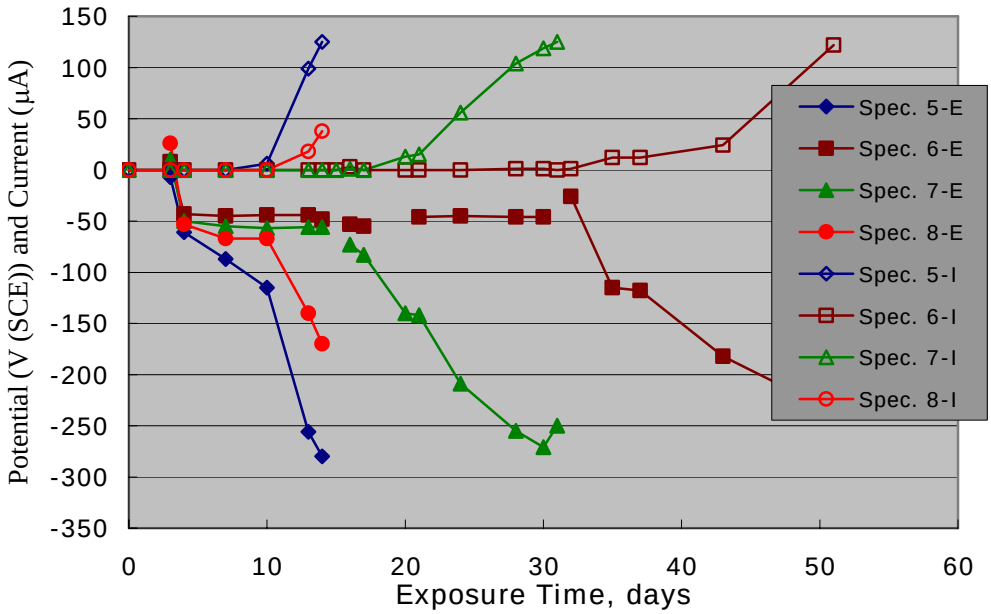

Figure 27: Potential and macro-cell current data for Specimens 5-8.

parameters were responding to corrosion activation, irrespective of agreement between the criteria.

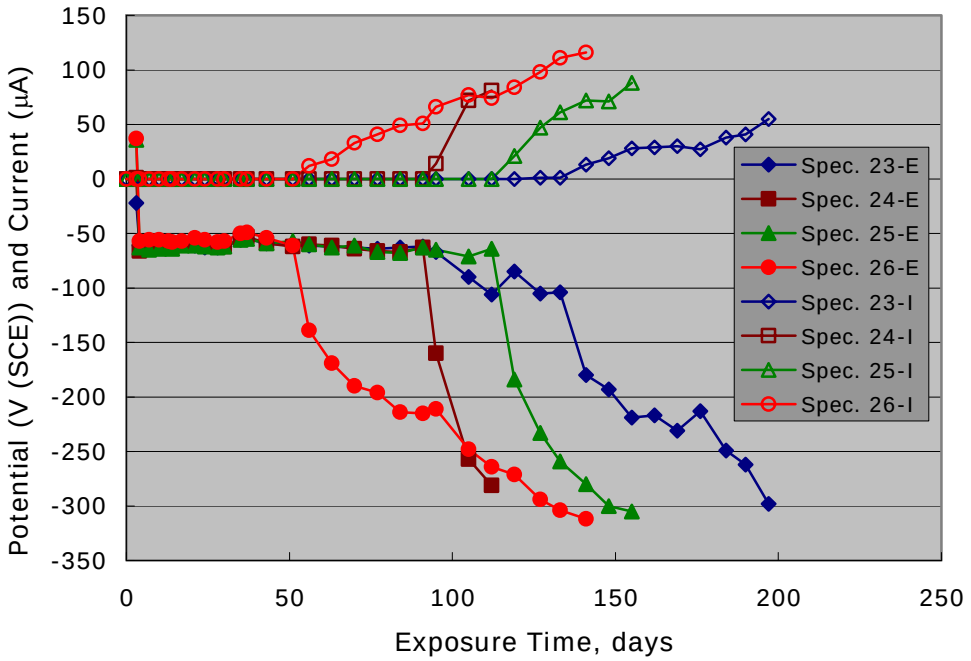

Figure 28: Potential and macro-cell current data for Specimens 23-26.

Figure 29 presents a Weibull cumulative distribution function (CDF) plot of time-to-corrosion according to each of the two criteria for all specimens of the LA0.50 mix design and exposure condition C1. The two representations are in general agreement in that 1) each indicates little or no difference in T_i for the as-received (AR) versus wire brushed (P) bars, 2) the mean T_i (eta) for the HA specimens exceeds that for the LA ones by a factor of about six, and 3) the data spread (beta) is generally the same with values in the approximate range of 2-4. Likewise, Figure 30 shows a similar representation for each of the four exposure conditions (see Table 4). This indicates general agreement between the two T_i representations (potential and macrocell current criteria) but with the latter displaced to lower T_i by about 30 percent at the mean. Also apparent is that the 40°C, 80 percent RH (C3) exposure (see Figure 24) resulted in the shortest T_i, C1 (20-22°C, 40-60 percent RH, Figure 22)) the highest, and with C2 (20-22°C, 80 percent RH, Figure 23) and C0 (outdoors, Figure 26) being intermediate and comparable. Representations of the HA0.37 specimen T_i's are not presently possible, as corrosion has not initiated in any specimens of this type.

Figure 31 shows a Weibull CDF of time-to-corrosion plot for LA specimens of both w/c (0.37 and 0.50) and each of the two reinforcement surface conditions

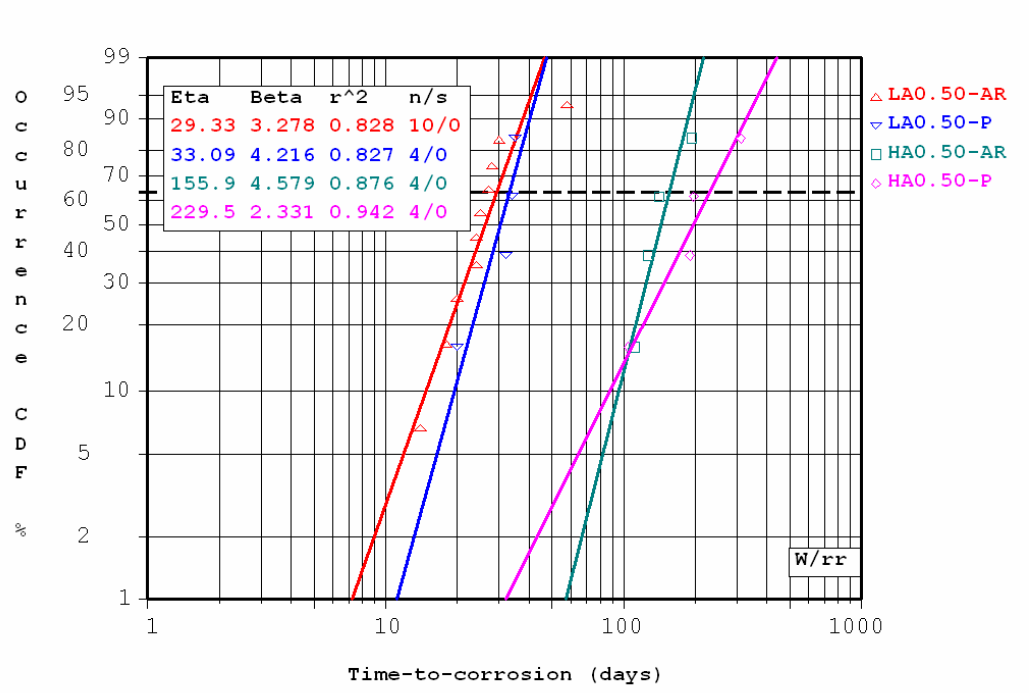

(a)

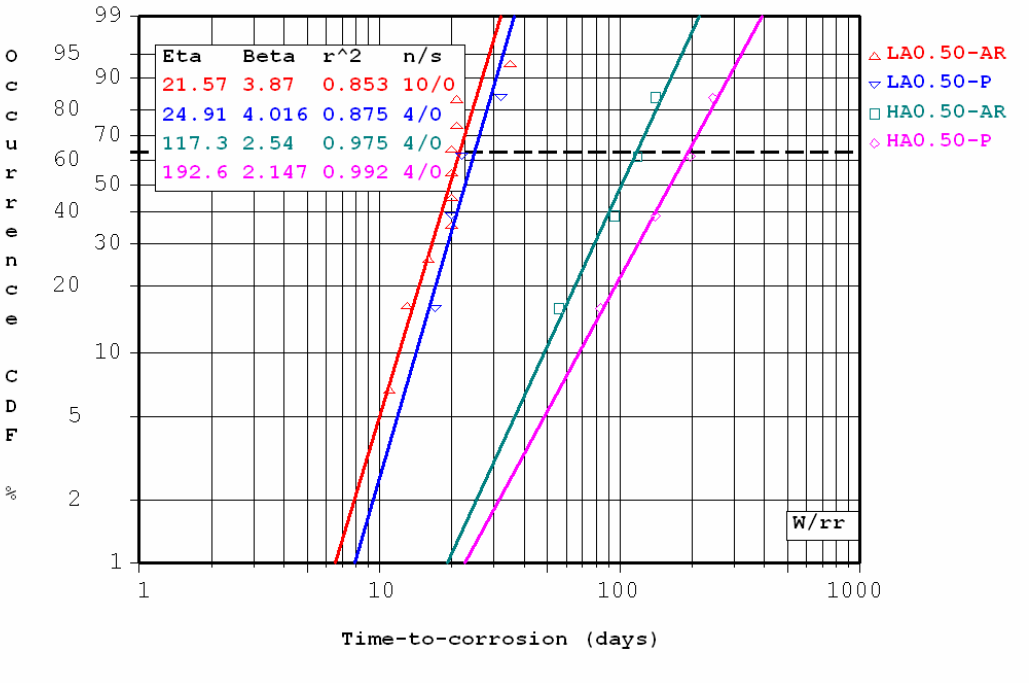

(b)

Figure 29: Weibull cumulative distribution function (CDF) of time-to-corrosion for LA0.50 specimens and exposure condition C1 according to the (a) potential criterion and (b) macrocell current criterion.

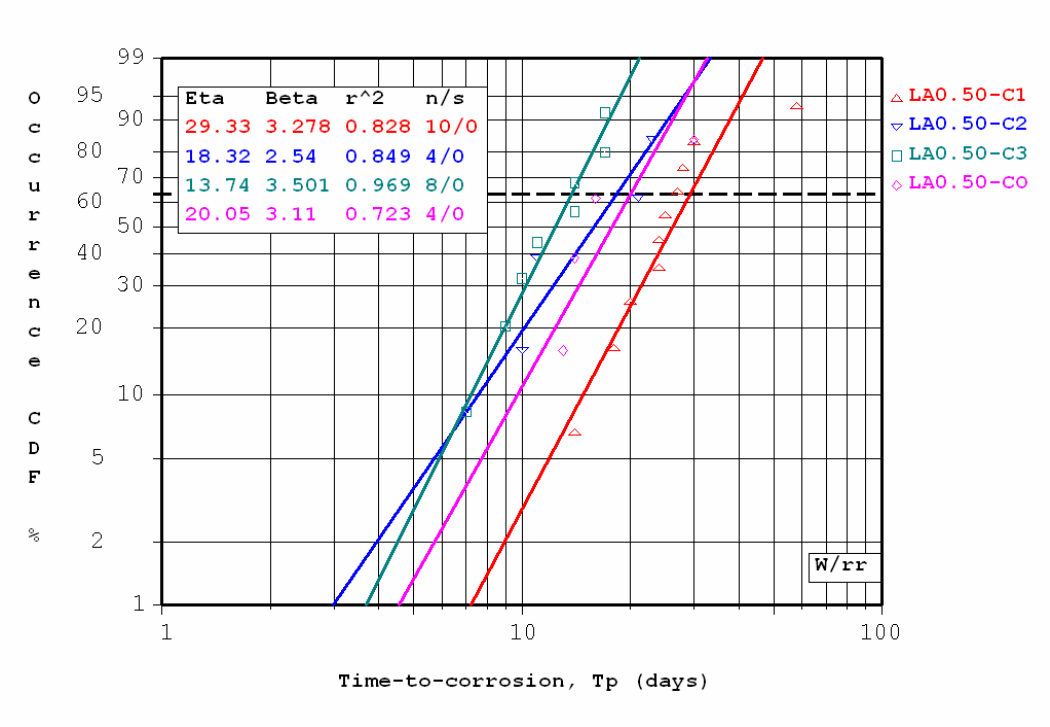

(a)

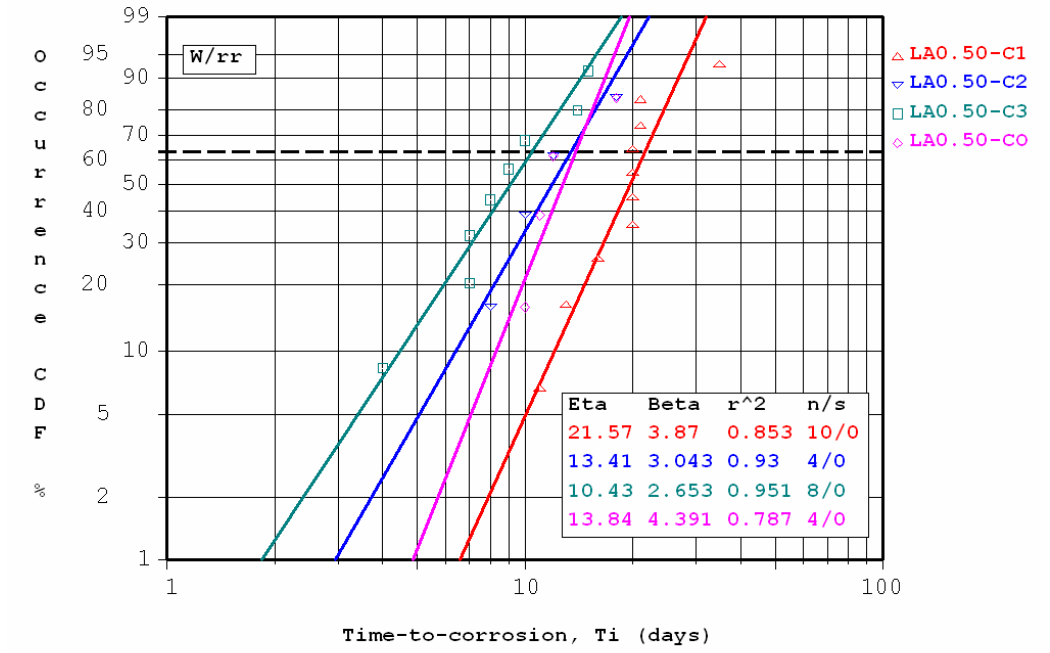

(b)

Figure 30: Weibull cumulative distribution function (CDF) for time-to-corrosion of LA specimens exposed under each of the four conditions (see Table 4) according to the (a) potential criterion and (b) macrocell current criterion.

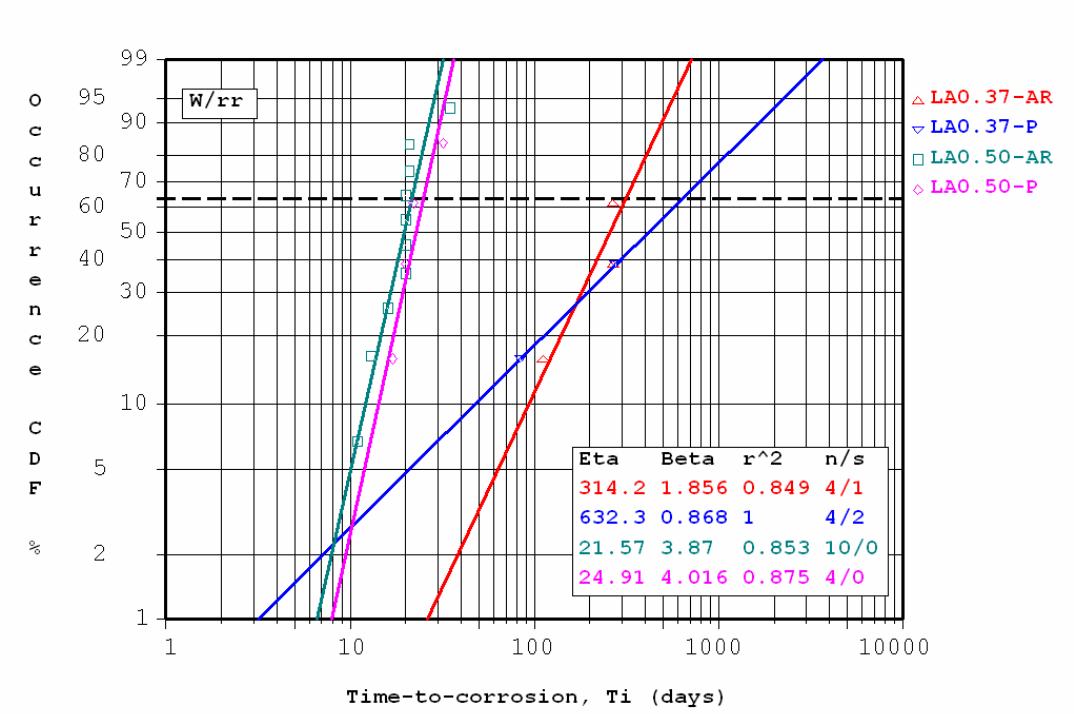

Figure 31: Effect of w/c and reinforcement surface condition on the CDF of T_I for the LA mix design specimens according to the macrocell current criterion.

according to the macrocell corrosion initiation criterion (insufficient specimens are presently active for analysis according to the potential criterion, see Table 7). Considering the limited w/c = 0.37 data, no distinction is indicated between the two bar conditions but with the mean LA0.37 T_I values being more than an order-of-magnitude greater than for the LA0.50 specimens. Exposure and data acquisition for specimens that are not yet active is continuing.

Figure 32 provides a comparison of T_i for specimens from the earlier project[22,23] (O) and those of the present (N). This indicates that the difference in T_i is relatively modest for the HA0.50 specimens (42 percent difference in eta) but that eta for the old LA0.50 ones exceeds that for the new by a factor of four. No explanation is apparent for this.

Table 9 presents analysis results for chlorides, both as-measured and corrected, based upon powder drilled from shallow depths along the top of the upper bar trace at passive locations after the specimen was broken open. The as-measured values were corrected by multiplying by T_I / T_A as an approximate means of accounting for

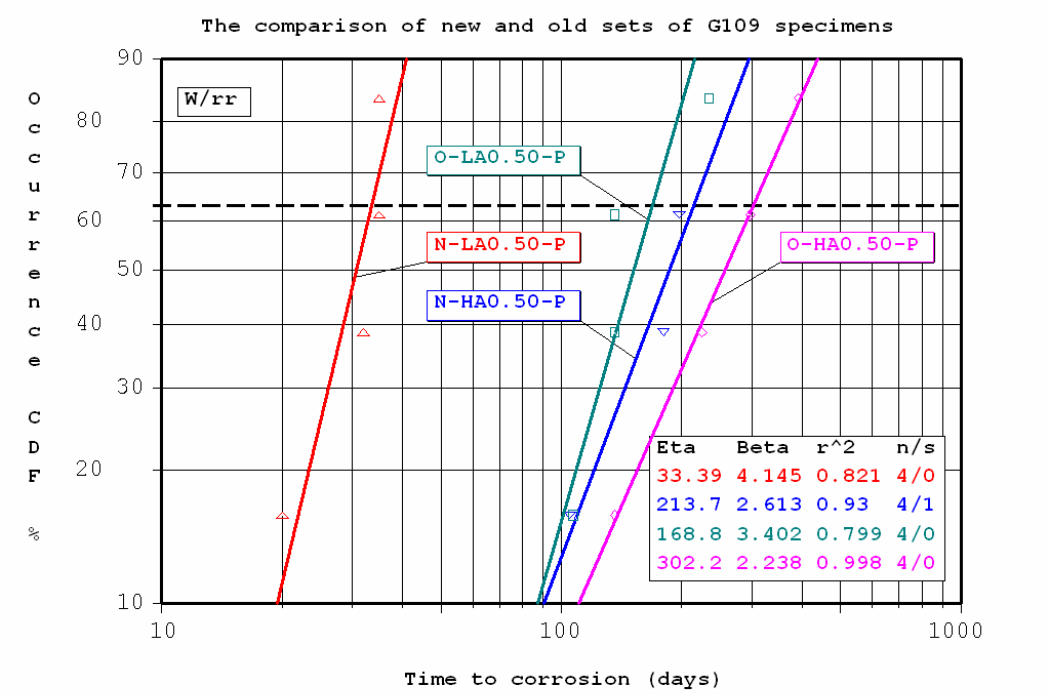

Figure 32: Weibull cumulative distribution (CDF) of time-to-corrosion plot for specimens of the previous (O) and present (N) programs.

the fact that T_A exceeded T_I in some cases such that chlorides continued to accumulate after corrosion initiated. The corrected [Cl^-] was taken as c_{th}. Figure 33 shows a Weibull distribution for c_{th} so determined in the case of the LA0.50 and HA0.50 mix designs for both bar surface conditions (as-received (AR) and wire brushed (P)). The limited data for the LA0.50-P, HA0.50-AR, and HA0.50-P are such that caution must be exercised in drawing conclusion; however, it appears that the mean c_{th} was slightly higher for the P compared to AR surface condition. Overall, there is a factor of two difference in the mean (eta); and except for the HA0.50-P specimens, the data spread (beta) is generally the same. Figure 34 indicates how c_{th} for the LA0.50 specimens varied with exposure with the C0 and C1 conditions exhibiting mean (eta) values about a factor of two less than for C2 and that for C3 being intermediate.

As noted above, the North American concrete literature typically cites c_{th} as about 0.77 kg/m^3 (1.3 pcy) on a concrete weight basis; however, FDOT experience has indicated 1.2-3.5 kg/m^3 (2-6 pcy). Obviously, the measured values from both the current and past programs are in excess of these. However, the data in Figures 33 and 34 indicate a c_{th} at one percent probability of occurrence of 0.3-2.3 kg/m^3

Table 9: Chloride concentrations at the upper rebar trace.

Specimen No.	Mix Design	Exposure	Cl^-, kg/m^3 (measured)	Cl^-, kg/m^3 (corrected)
1	LA0.50-AR	C1	10.61	7.96
2			8.67	6.19
3			8.49	6.47
4			4.42	2.90
5			4.70	3.69
6			10.01	6.04
7			8.04	5.03
8			2.42	2.25
9			6.47	4.62
10			6.60	4.71
11	LA0.50-P		9.70	6.10
12			9.07	4.41
13			8.14	7.75
14			15.88	14.52
23	HA0.50-AR		14.35	10.27
24			6.67	5.66
25			10.01	7.69
26			14.38	5.71
27	HA0.50-P		22.01	22.01
28			4.10	3.04
29			22.14	17.44
30			17.14	12.27
39	LA0.50-AR	C2	14.24	12.95
40			21.72	12.41
41			6.29	5.59
42			12.13	7.80
43		C3	10.56	8.64
44			8.58	6.67
45			11.31	5.66
46			11.49	8.94
47			7.29	6.43
48			9.67	7.96
49			5.78	5.14
50			4.48	4.07
51		CO	8.59	5.52
52			4.77	4.37
53			3.78	3.24
54			5.44	3.89

(0.6-3.9 pcy) and at ten percent probability 2.3-4.4 kg/m^3 (3.9-7.5 pcy). These c_{th} ranges are in general accord with the Florida experience, considering that corrosion

induced substructure damage on the order of ten percent is likely to be noted on Bridge Inspection Reports

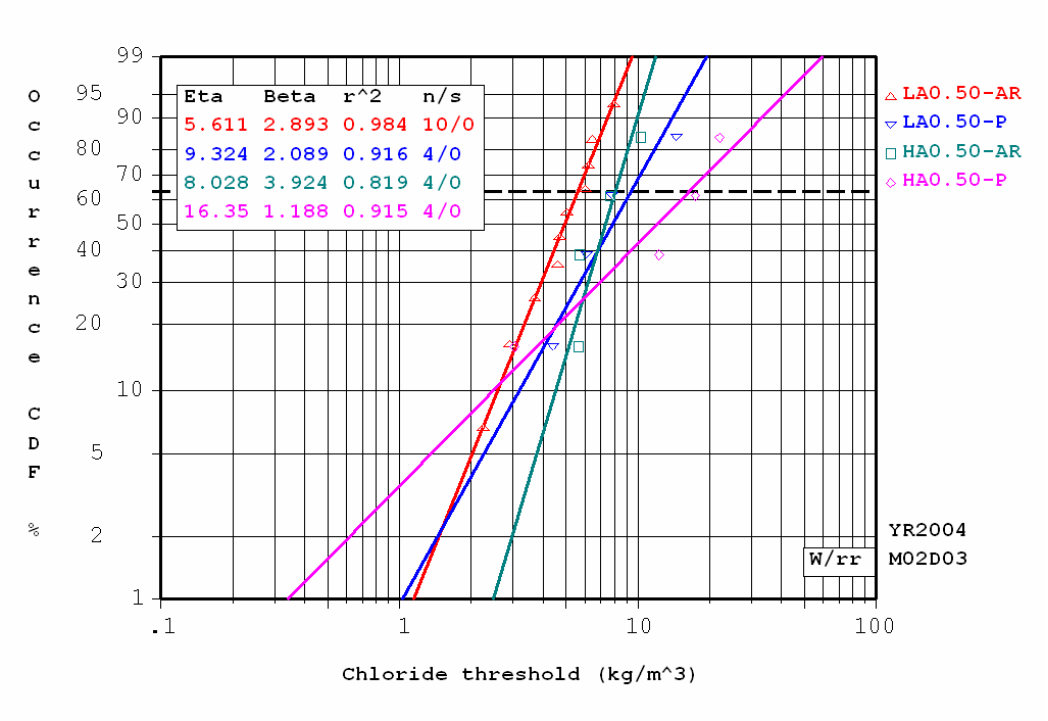

Figure 33: Weibull cumulative distribution (CDF) for C_{th}.

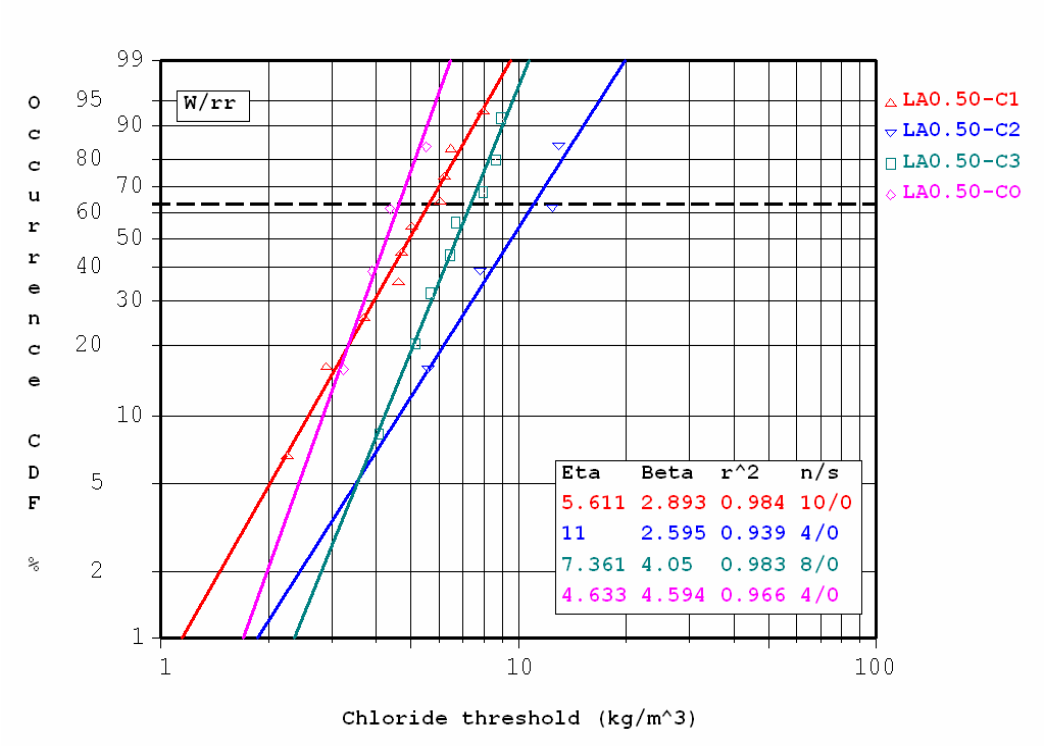

Figure 34: Weibull cumulative distribution (CDF) for c_{th}, as measured for specimens that underwent the different types of exposure.

Figure 35 plots c_{th} as a function of time for the C1 exposures. Unlike the results from the previous program[22,23] (Figure 12), these data do not obviously conform to a common trend and, instead, have been represented as two separate distributions, each of which has been fitted by a straight line. The trend line from the previous results is also indicated for comparison. Absence of a common trend may have resulted because only LA and HA cements were used in the present program, whereas LA, NA, and HA were employed in the previous, thus better facilitating a progressive transition in c_{th} with increasing T_i. The present results are consistent with the previous ones; however, in that c_{th} varied in proportion to exposure time. The fact that both straight lines approximately extrapolate to the origin is consistent with sorption having been a primary contributor to Cl^- uptake, as projected above, whereas results from the first specimen set are more consistent with predominance by diffusion. The time variation for corrosion initiation in the two programs may have caused this difference.

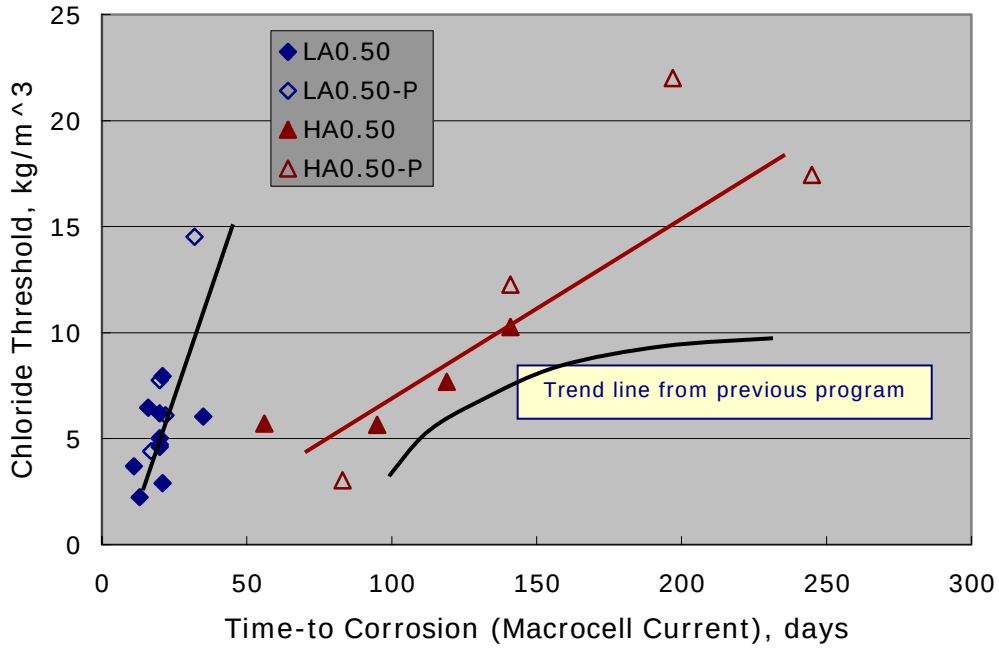

Figure 35: Plot of chloride corrosion threshold versus time-to-corrosion.

Specimen Type 2

The onset of active corrosion for the 8X, 4X, and 2X specimens occurred after 45, 50, and 55 days, respectively, according to the potential criterion and 28, 30, and 37 days, respectively, according to the macrocell current one. This ordering is

consistent with greater bar surface area promoting reduced T_i. Subsequently, a second set of data was collected by inverting these specimens and repeating the experiment by ponding what was initially the bottom specimen surface. In this case, macrocell data could not be collected because the formerly top bars were already active. Also, the top exposed surface was ponded with tap water for two weeks prior to salt solution application in an effort to reduce sorptive salt solution uptake. Table 10 presents the T_i data for both exposures, and Figure 36 shows the potential criterion results graphically. This indicates that T_i, first, varied inversely with the number of bars (alternatively, exposed steel surface area) in both experiments and, second, was greater for the second experiment than the first. The latter observation is consistent with the wetter state of the specimens during this exposure. However,

Table 10: T_i data for Type 2 specimens.

Experiment	Specimen Type	E_P	E_I
1	2X	56	37
	4X	50	30
	8X	45	28
2	2X	111	-
	4X	111	-
	8X	81	-

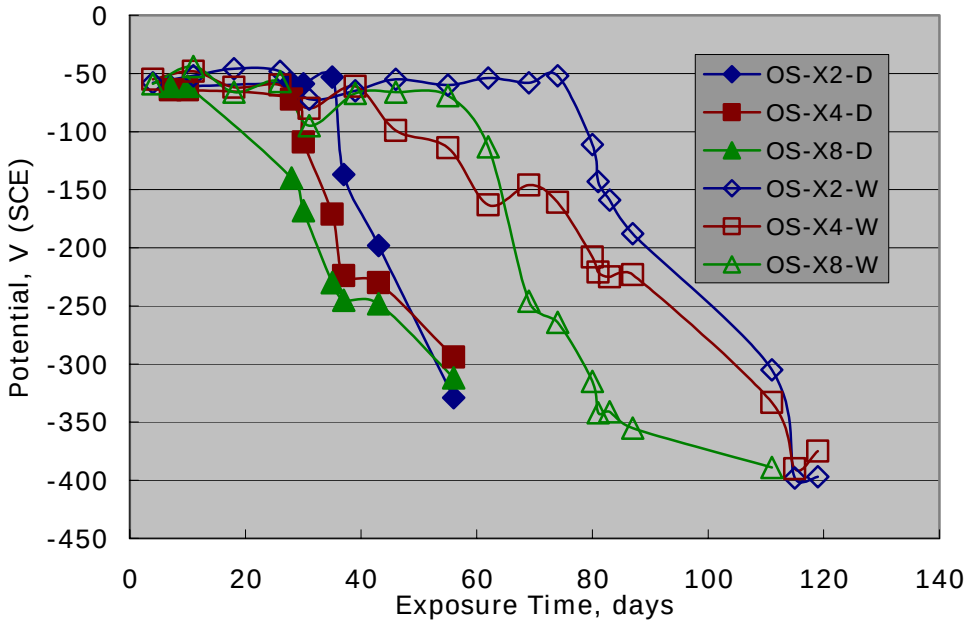

Figure 36: Potential as a function of exposure time for two experiments involving oversized G109 specimens.

comparison of these data with those of the Type 1 specimens (Table 7) of the same mix design (LA0.50) shows that bars in the Type 2 specimen became active in an overall shorter time than those in the Type 1. The reason for this is unclear.

Specimen Type 3

Table 11 provides T_P data for the Type 3 specimens. As for the Type 1, these are characterized by relatively short times to corrosion initiation for the higher w/c

Table 11: Time-to-corrosion data for Type 3 specimens.

Spec. No.	Mix Design*	Time-to-Corr., days	Spec. No.	Mix Design*	Time-to-Corr., days
1	LA0.50-CWL	13	25	LA0.37-P-TWL	>196
2		7	26		97
3		7	27		73
4		19	28	HA0.50-TWL	2
5		23	29		7
6		13	30		13
7		27	31		35
8		76	32		2
9		9	33		9
10	LA0.50-TWL	2	34	HA0.50-P-TWL	23
11		7	35		48
12		20	36		35
13		13	37	HA0.37-TWL	132
14		2	38		72
15		23	39		72
16	LA0.50-P-TWL	20	40		85
17		13	41		97
18		13	42		114
19	LA0.37-TWL	76	43	HA0.37-P-TWL	171
20		16	44		35
21		41	45		>196
22		114			
23		30			
24		35			

* P: polished surface condition.
* TWL: tidal water level.
*CWL: cyclic water level.

specimens and for the LA compared to HA concretes. Figures 37-40 present Weibull CDF plots of T_i that show the effect of the different variables represented in this test matrix. Thus, Figure 37 indicates that shorter times-to-corrosion occurred for specimens exposed to the cyclic (TWL) compared to constant (CWL) water level condition. Figures 38 and 39 indicate the effect of cement alkalinity, the former for w/c 0.50 specimens and wire brushed (P) surface preparation and the latter for both w/c's and as-received (AR) surface condition. The TWL exposure applies to both data sets. The former plot (Figure 38) indicates an increase in the mean time-to-corrosion (eta) for the HA versus LA specimens by a factor of 2.5, while the latter (Figure 39) indicates no difference for the same w/c and cement alkalinity. This suggests that for this w/c the normal benefit of a HA versus LA cement was nullified by the poorer (AR compared to P) surface condition. On the other hand, the w/c 0.37 specimen data in Figure 40 indicate a 2.5 times greater time-to-corrosion for the HA compared to LA specimens. The fact that corrosion commenced after just two days in some cases indicates that the results may not have long-term applicability. Also, some of the specimens that have been autopsied to-date have had bar misalignments such that cover was not constant.

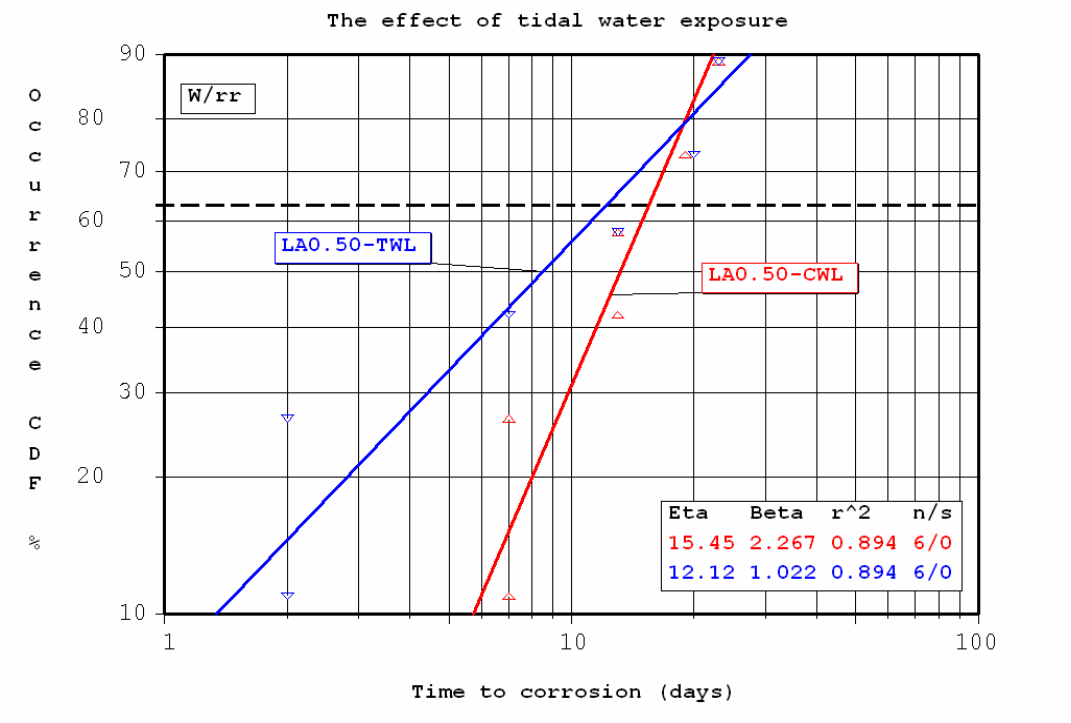

Figure 37: Effect of cyclic versus constant water level (TWL and CWL, respectively) on T_i for Type 3 specimens.

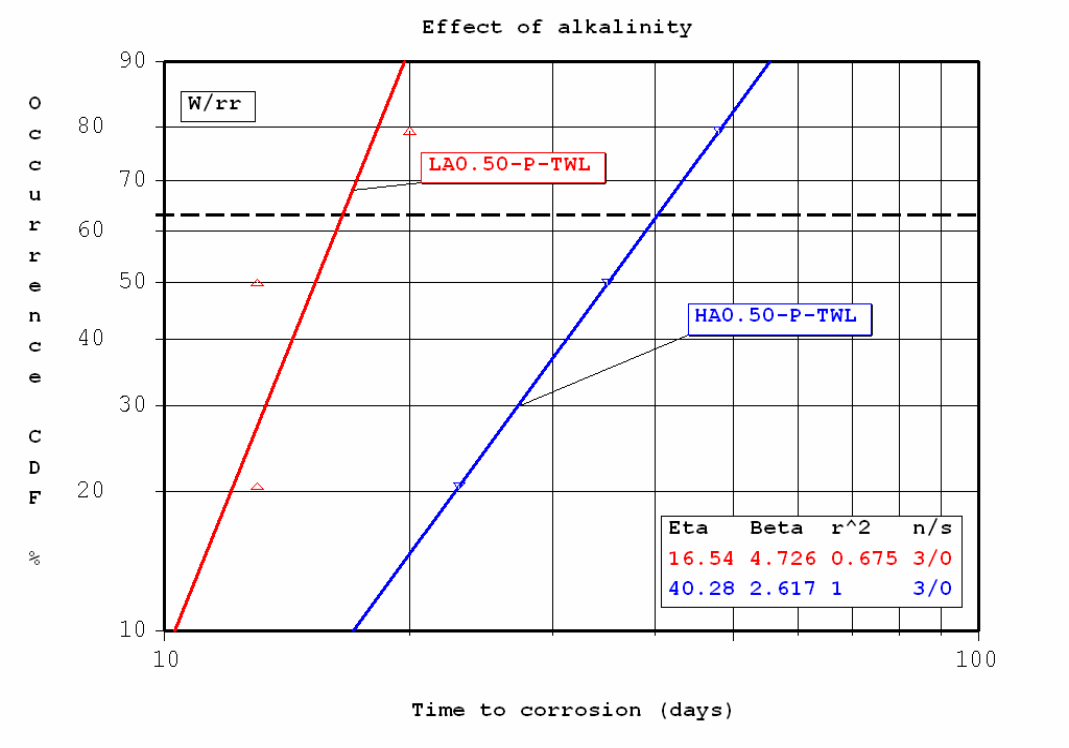

Figure 38: Effect of cement alkalinity on T_i for Type 3 specimens.

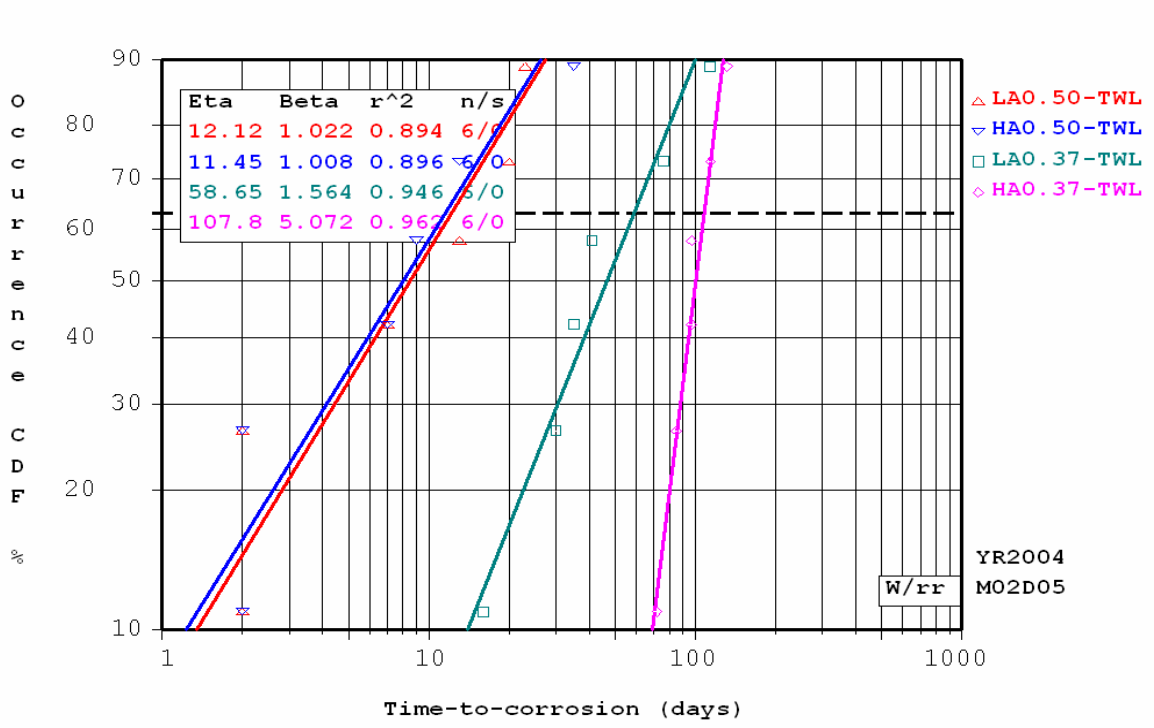

Figure 39: Effect of w/c on T_i for Type 3 specimens.

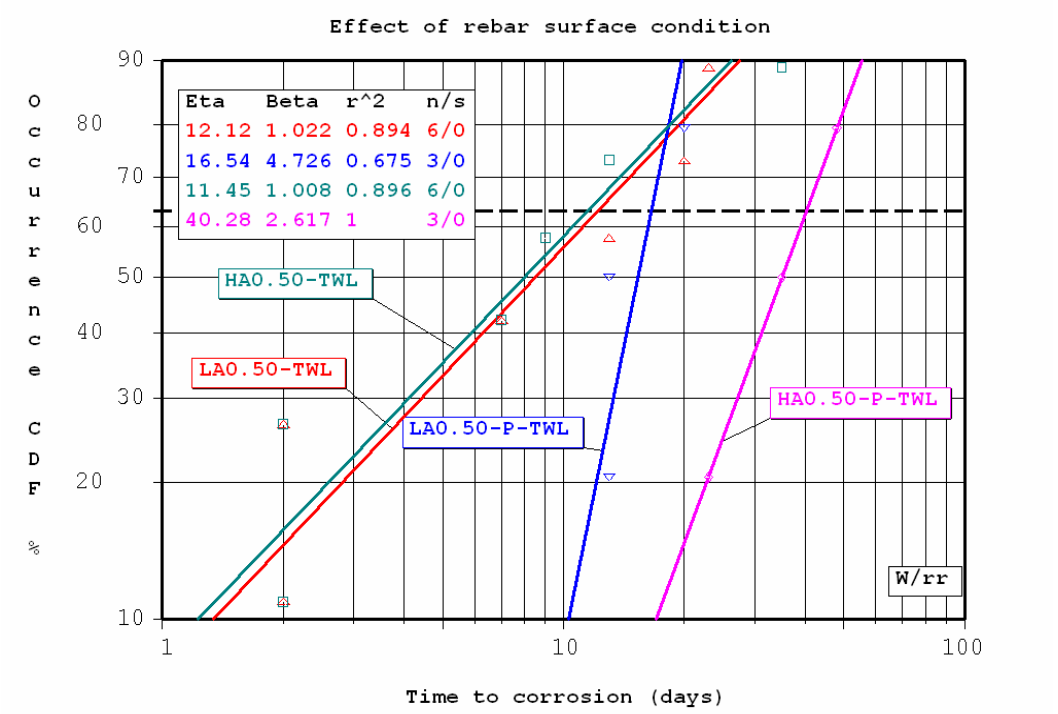

Figure 40: Effect of bar surface condition on T_i for Type 3 specimens.

Preferential Corrosion Initiation at Air Voids

Background

Several previous research studies, as well as the preceding project,[22,23] have reported that corrosion initiated preferentially at air voids at the rebar surface. In an attempt to further study and understand this phenomenon, an analysis was performed of air voids in the present specimens. To do this, Type 1 Specimens 1-10 and 23-26 (see Table 7) were selected for further analysis. As noted above, T_I for the HA specimens exceeded that for the LA ones by approximately six-fold.

The autopsies revealed a single or several locally corroded regions on the top of the upper bar for all specimens. In cases where the time difference between T_I and T_A was relatively large compared to T_I, the corrosion was more advanced. On the other hand, corrosion was modest where the difference between these two times was small. This indicates that the macro-cell current increase corresponded to the onset of corrosion and that this corrosion progressed with time.

Figure 41 shows a photograph of the rebar trace at the corrosion initiation site for Specimen No. 5, which was autopsied shortly after corrosion initiated. Correspondingly, Figure 42 illustrates a case where this time difference was relatively large (Specimen No. 7). Here, corrosion products are more extensive than in Figure 41. Note that in both cases air voids are present along the rebar trace, including at the corrosion site.

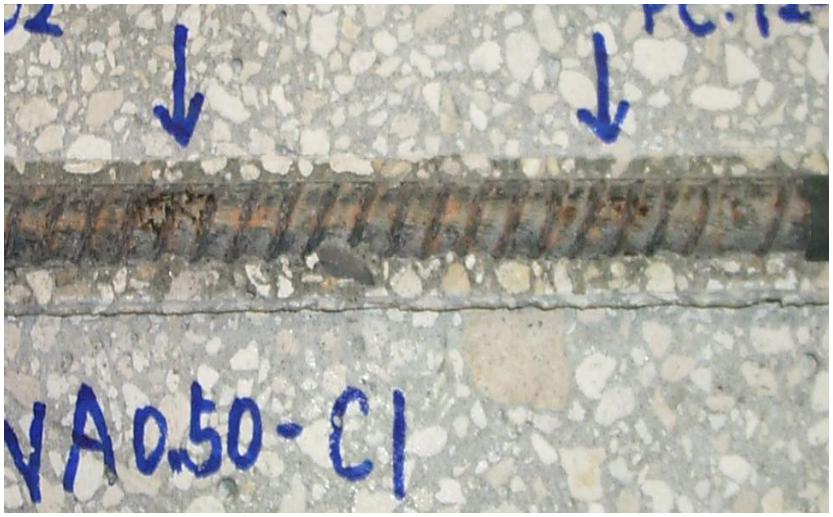

Figure: 41 Photograph of corrosion on the rebar of Specimen No. 5.

Figure 42: Photograph of corrosion on the rebar trace of Specimen 7.

Air Void Distribution on the Upper Rebar Trace

Entrapped air voids in concrete are generally spherical with a diameter larger than one mm. Characterization of the size and distribution of air voids along the top of the upper bar trace was based upon a diameter measurement assuming the voids were half spheres or ellipsoids. In the latter case (ellipsoids), the diameter was taken as the arithmetic mean of the two major axes. Figure 43 shows a photograph of a bar trace with various voids identified according to size.

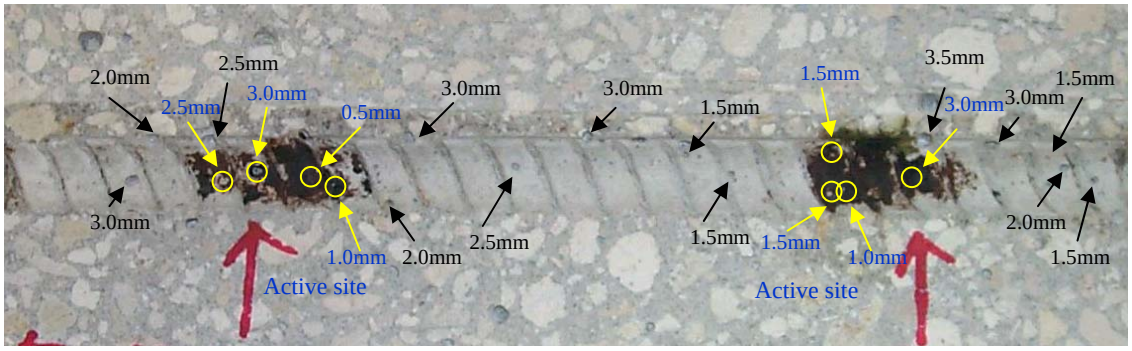

Figure 43: Photograph of an upper bar trace with various air voids identified both at the corrosion site and elsewhere.

Figure 44 shows a plot of the average cumulative number of voids 0.5 mm in diameter and larger per LA and HA specimen as a function of void diameter. It is apparent from this that there was a greater number of voids along the bar trace for the HA compared to LA concrete. Also, void size in the HA specimens extended to greater diameters. It is not known if this was a consequence of the nature of HA compared to LA cement concretes or if this reflects inadvertent variations in different concrete batches.

Figure 45 presents a plot of, first, the average cumulative number of voids (percent basis) per specimen along the entire bar trace versus void diameter and, second, maximum void size at the corrosion site (cumulative percent basis also) versus void diameter for both the LA and HA specimens. This indicates that one or more voids was present at the initiation site for 12 of the 14 specimens (no voids were apparent at the corrosion site for two of the ten LA specimens). For both pairs of distributions, the active site ones begin at and are displaced toward greater void diameter than are the total ones, with the trend being more definitive in the HA specimen case. This suggests that the tendency for corrosion initiation increased in

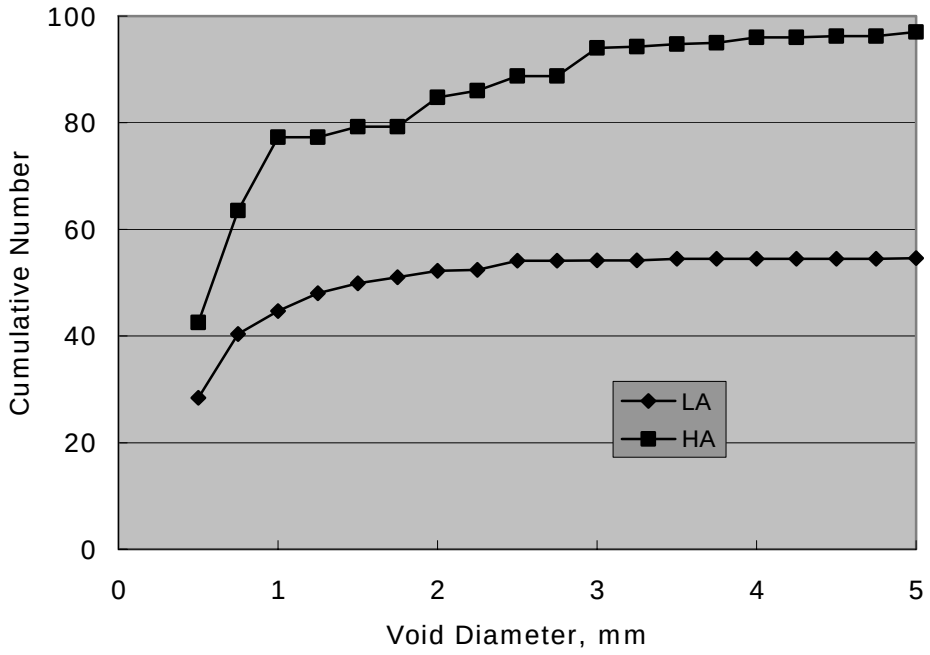

Figure 44: Average cumulative number of voids along the rebar trace per specimen as a function of void size.

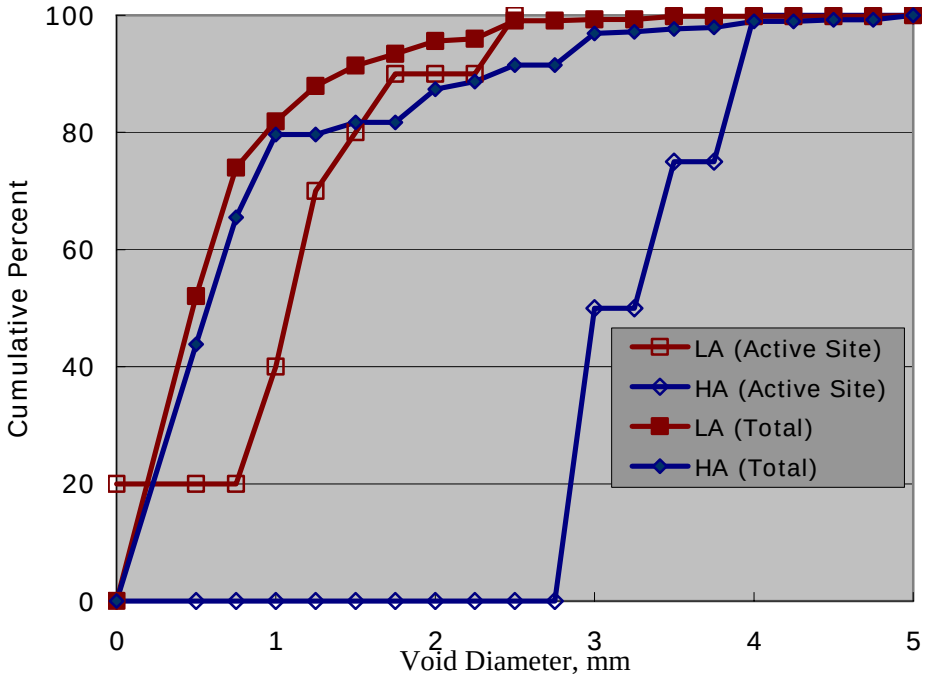

Figure 45: Cumulative distribution of diameter for 1) all voids along the upper bar trace and 2) the maximum void at the corrosion site for LA and HA specimens.

proportion to void diameter with the trend being modest for the LA concrete and relatively pronounced for the HA. Likewise, Figure 46 provides a similar representation as in Figure 45 but for as-received versus wire brushed HA specimens. The data indicate that the total void distribution was approximately the same for both bar surface conditions but that voids of a given size in the wire brushed (P) specimens were more resistant to corrosion initiation than were ones in the as-received (AR). This finding is consistent with the projection that c_{th} was greater for the P compared to AR specimens (Figure 33).

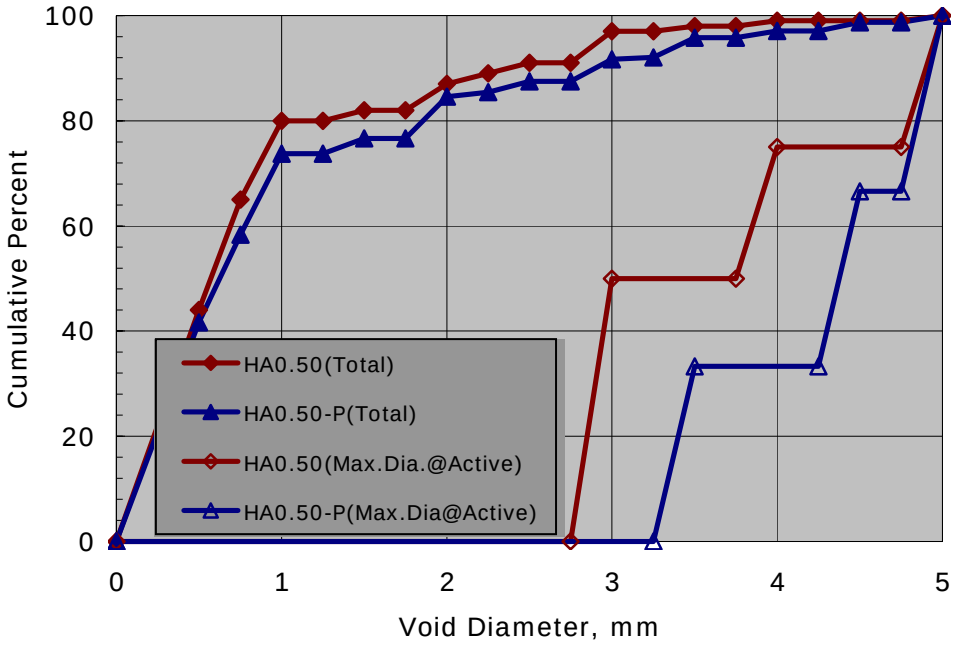

Figure 46: Average cumulative distribution of all voids according to size and of the maximum void size at corrosion sites for as-received (no designation) and wire brushed (P) specimens of the HA0.50 mix design.

Figure 47 provides yet another representation of the void size effect upon corrosion initiation as a plot of the ratio of the number of voids at the active site (V_a) to the total number of voids (V_t) versus void size. No dependence of V_a/V_t is apparent for the LA0.50 mix design specimens, but for the other three cases, the ratio increased progressively with increasing void diameter. No correlation was apparent between maximum void size and T_i.

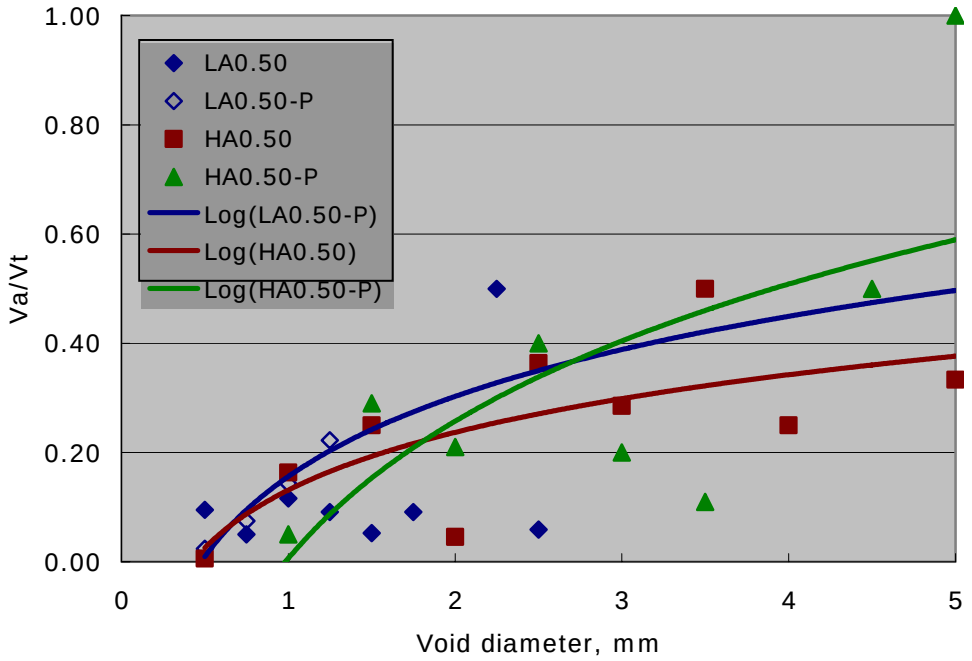

Figure 47: Plot of the ratio of the average number of voids at active sites to the total number of voids (V_a/V_t) as a function of void size per specimen.

Effect of Relative Humidity and Temperature on the Effective Diffusion Coefficient

Relative Humidity

Figure 48 reports the RH record for the four controlled chambers (Figure 19) as well as for the ambient laboratory air. This indicates that the target values (RH = 35, 55, 75, and 95 percent) were reasonably maintained. Likewise, Figure 49 shows RH data as recorded from the internal concrete probes. In all cases the internal RH was greater than that of the respective chamber, the effect being more pronounced the lower the chamber RH. This is due in part to RH enhancement from the salt water spraying of the exposed surface. Spraying of the top surface of these specimens commenced 112 days after exposure.

Figure 50 shows the measured Cl^- profiles for a second set of concrete specimens exposed to constant RH and for one specimen that was alternated between RH 35 and 95, as determined after 180 days of spraying the top surface

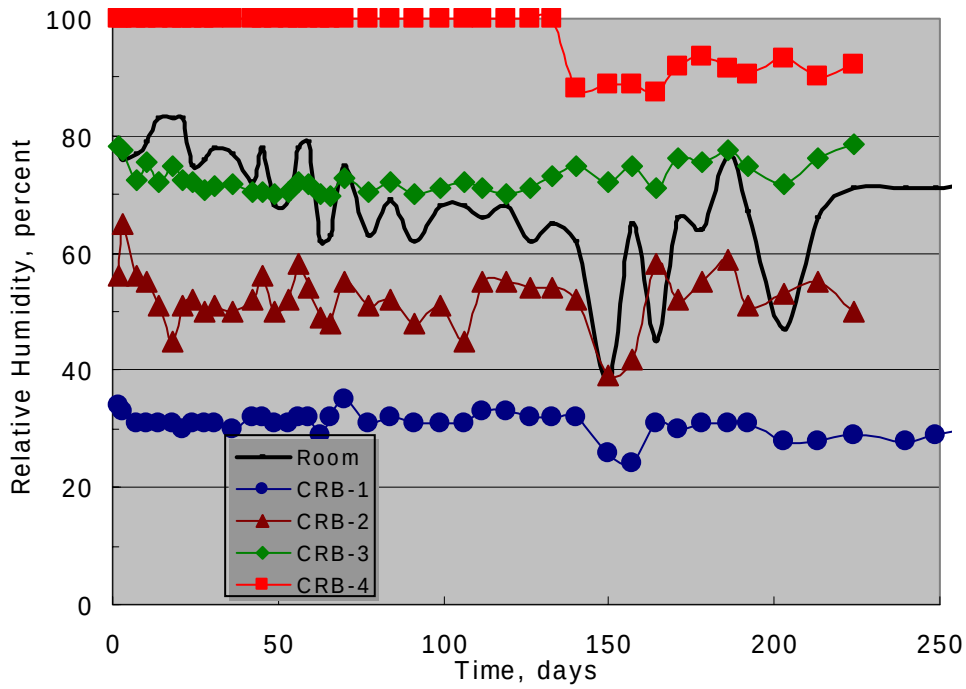

Figure 48: Relative humidity record for the four control chambers and the ambient laboratory.

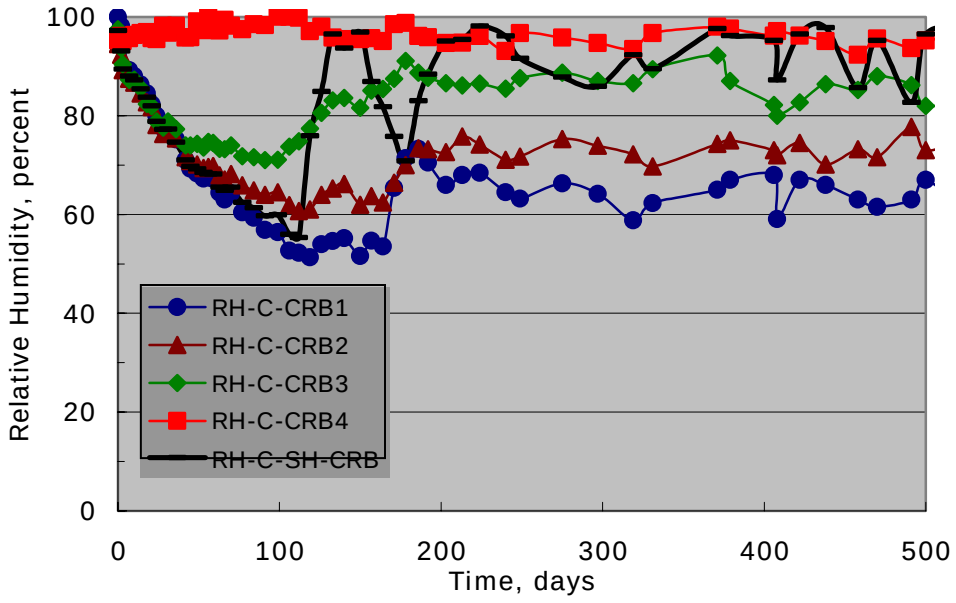

Figure 49: Internal concrete relative humidity record for specimens in each of the four control chambers as well as for the specimen that was switched between the RH 35 and 95 chambers (RH-C-SH-CRB).

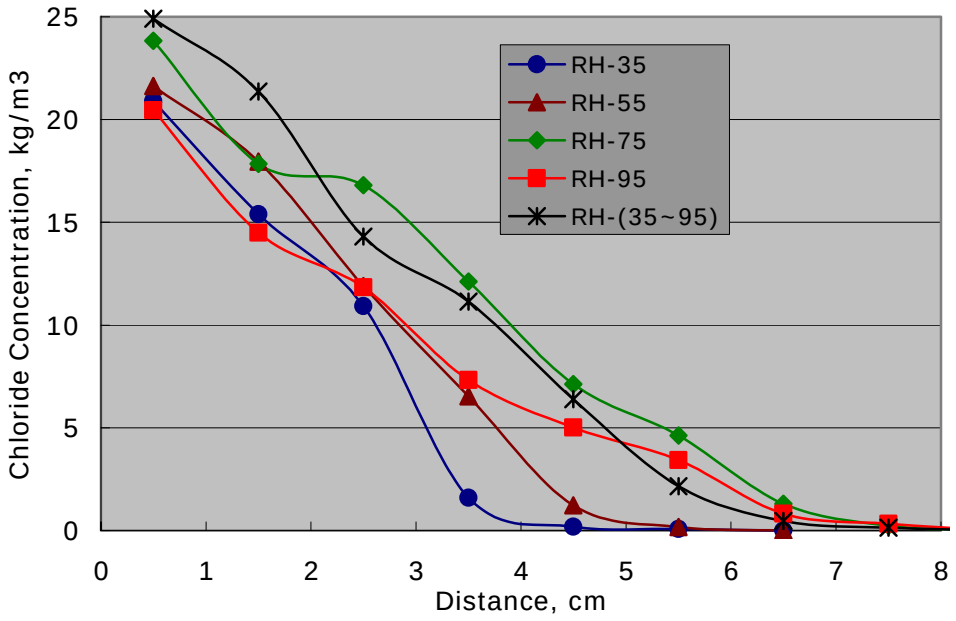

Figure 50: Chloride profiles for specimens exposed to constant RH and for alternation between RH 35 and 95.

with a 15 w/o NaCl solution. Each conforms to an approximately straight line with slightly different slope and variations in surface concentration (C_s). As such, the data are not purely Fickian and probably reflect an influence of sorption and Cl^- binding. Figure 51 shows a typical [Cl^-] – depth curve fitting plot from which D_{eff} was calculated. In this case, the initial two data points fall below the best-fit curve,

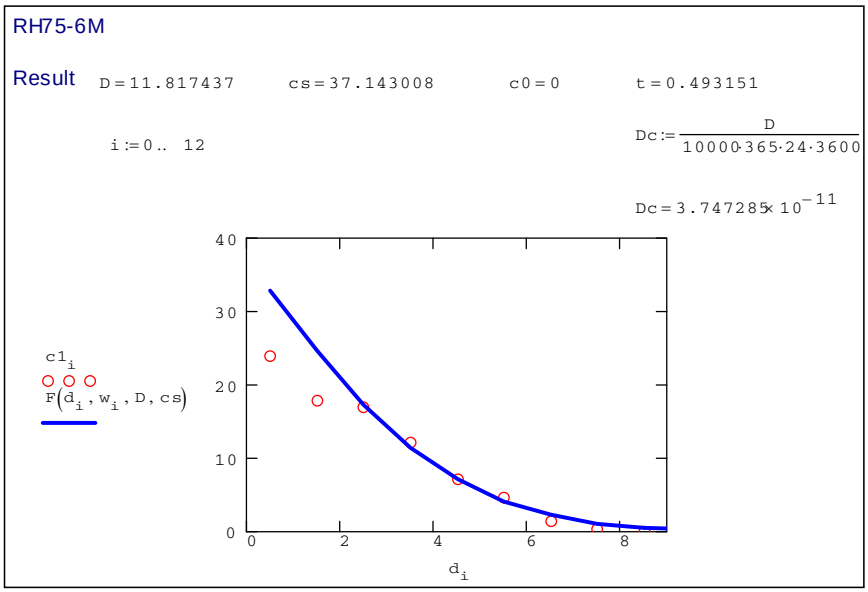

Figure 51: Fickian curve fit to the RH 75 [Cl^-] data (C_s = 37.14 pcy (21.91 kg/m^3), t = 0.49 years, D_{eff} = 3.75·10^{-11} m^2/s (11.82 cm^2/y)).

suggesting that carbonation combined with release of bound Cl^- may have occurred. As a reanalysis that attempted to account for this, these data were evaluated without the first two points and with the depth scale adjusted accordingly. Figure 52 shows the curve fit and results from doing this and that agreement between the data and curve is improved over that in Figure 51. Correspondingly, Figure 53 presents D_{eff} results according to, first, inclusion of all [Cl^-] data and, second, selective exclusion of the first several data points. This shows that the former method yielded higher D_{eff} than the latter because inclusion of the shallow depth [Cl^-] data tended to flatten the profile. The two D_{eff} values at 95 percent RH are identical because the fit was good with all data included, as shown by Figure 54. This presumably resulted because the high RH minimized sorption and carbonation. The D_{eff} for the specimen that was cycled between RH 35 and 95 was intermediate to the value at each of these extremes and is approximately the same as that at the average RH (65 percent). This suggests that RH variations did not significantly alter Cl^- intrusion rate or profile.

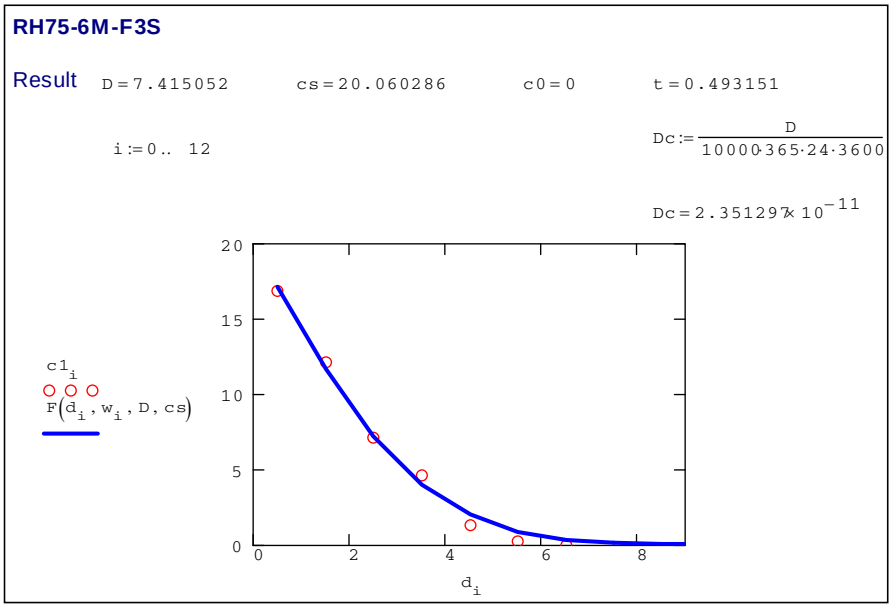

Figure 52: Fickian curve fit to the RH 75 [Cl^-] data with initial two data points eliminated (C_s = 20.06 pcy (11.84 kg/m^3), t = 0.49 years, D_{eff} = 2.35·10^{-11} m^2/s (7.42 cm^2/y)).

Temperature

Figure 55 shows Cl^- profiles at each of four constant temperatures and for a specimen that was cycled between 20 and 40°C (Specimen No. TS). The data show

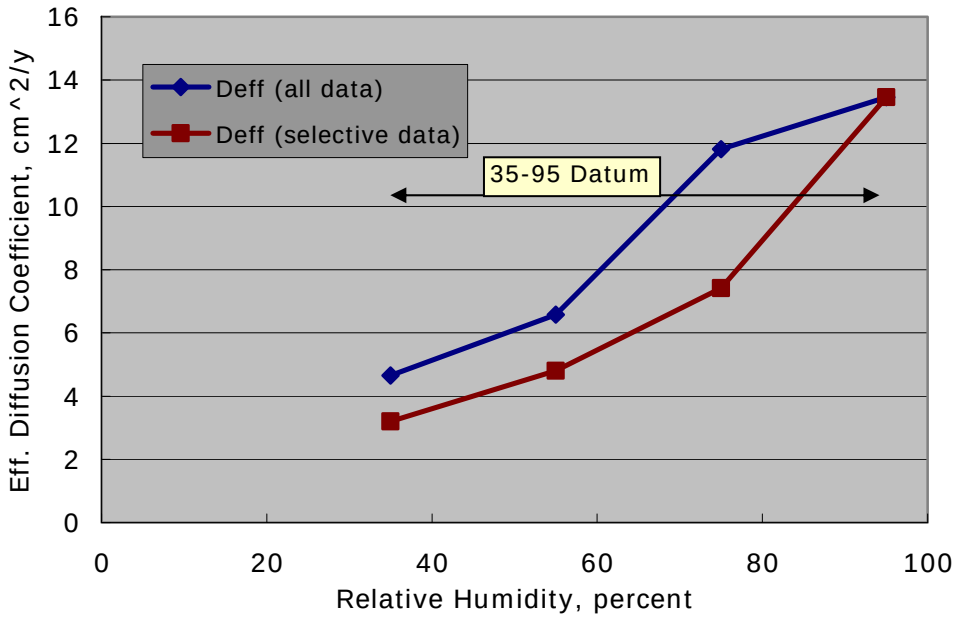

Figure 53: Calculated values of the effective diffusion coefficient as a function of RH.

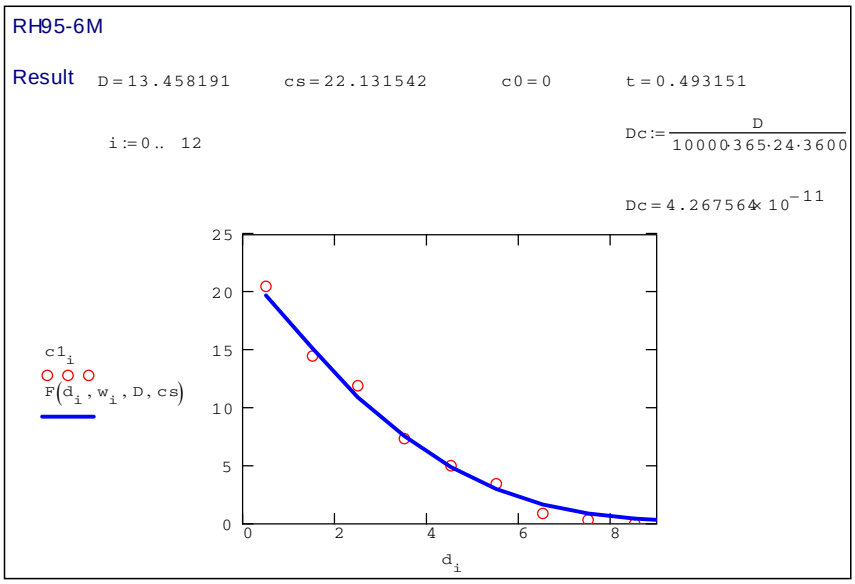

Figure 54: Fickian curve fit to the RH 95 [Cl^-] data.

an intermediate maximum at 2-3 cm depth in all cases except for the 0°C specimen. Also, surface concentration was highest for the cycled specimen and lowest for the 0°C one.

As for the Cl^- profile data as a function of RH, the constant temperature data

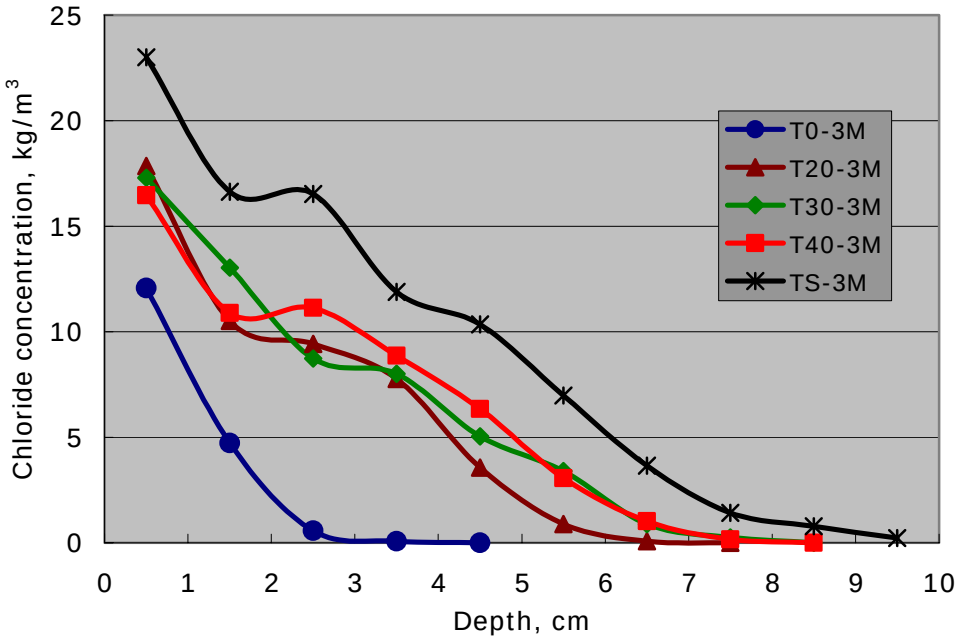

Figure 55: Chloride profiles as a function of temperature.

were also evaluated with and without the first several data points included. Figure 56 shows the resultant plot of D_{eff} versus temperature for each of these two cases. Because the data points at 0°C were limited, no attempt was made to edit these; and

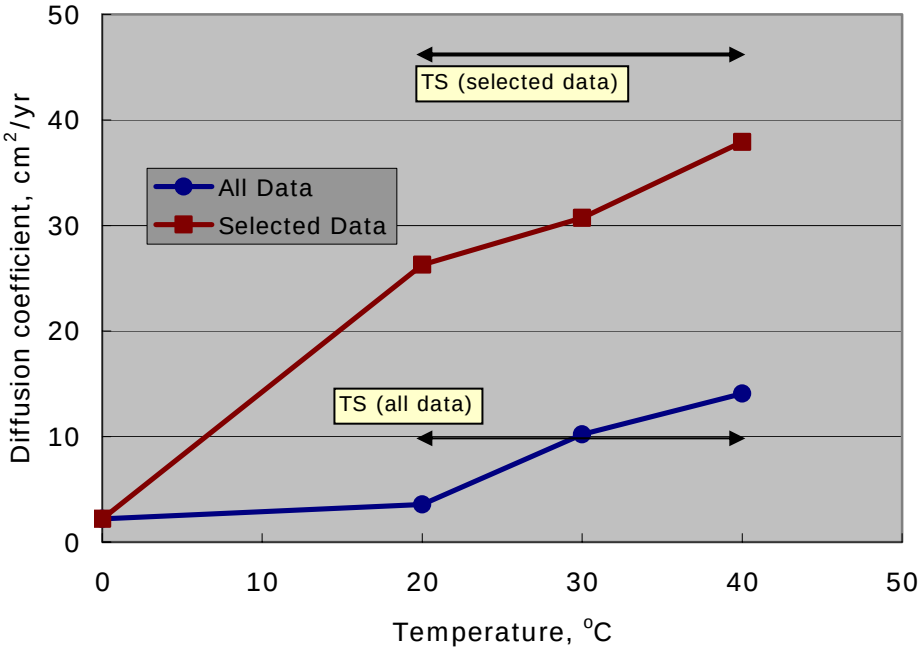

Figure 56: Effective diffusion coefficient as a function of temperature according to each of the calculation methods.

so D_{eff} is the same in both cases. Otherwise, there is a three-to-four-fold difference in the two sets of values. Also, in the analysis where near-surface data were edited, the thermally cycled specimen indicated a higher D_{eff} that that at even the higher temperature. This suggests that caution should be exercised in projecting Cl^- intrusion rates in service, where temperature variations are likely to occur, from laboratory data in cases where the latter are acquired at constant temperature.

CONCLUSIONS

A series of G109 specimens was exposed to cyclic NaCl solution ponding and simulated piling ones to continuous partial immergence; and time-to-corrosion was assessed based upon potential and macro-cell current measurements. Specimen variables included cement alkalinity (Na_2O_e of 0.317 and 1.078 (designated LA and HA, respectively)), water-to-cement ratio, w/c (0.50 and 0.37), and bar surface condition (wire brushed (P) and as-received (AR)). The following conclusions were reached.

1. Time-to-corrosion for the 0.50 w/c, HA G109 specimens exceeded that of the 0.50 w/c, LA specimens by a factor of six. Corrosion has not initiated for the w/c 0.37 HA specimens, and so comparisons cannot be made in the case of the lower w/c. Time-to-corrosion for w/c 0.37 LA G109 specimens, which have become active, exceeded that for w/c 0.50 LA ones by a factor of about 20.

2. The chloride threshold, which was projected from the concentration of this species along the top of the G109 upper bar trace upon specimen autopsy, increased in proportion to time-to-corrosion. Variations in concrete or steel (or both) composition and microstructure at the bar surface from one specimen to the next are thought to have caused time-to-corrosion and, hence, the Cl^- threshold to be a distributed parameter.

3. G109 specimens with wire brushed bars had slightly longer times-to-corrosion and higher chloride thresholds than ones with bars in the as-received condition.

4. The mean chloride concentration threshold for corrosion initiation for the present w/c 0.50, LA G109 specimens was in the range 5.5-9.2 kg/m^3 (9.3-15.6 pcy) on

a concrete weight basis. This exceeds by a factor of 7-12 the commonly referenced value in the north American concrete literature (0.77 kg/m^3 (1.3 pcy)). At the same time, FDOT experience has indicated a threshold of 1.2-3.5 kg/m^3 (2-6 pcy). Thus, the presently reported thresholds exceed this range by a factor of 1.5-8. However, the presently measured thresholds at one percent probability of occurrence were in the range 0.3-2.3 kg/m^3 (0.6-3.9 pcy) and at ten percent probability 2.3-4.4 kg/m^3 (3.9-7.5 pcy). These ranges are in general accord with the Florida experience threshold range listed above.

5. G109 specimens that were cyclically ponded at 40^{o}C had relatively short times-to-corrosion initiation compared to exposures at a) 80 percent relative humidity and ambient laboratory temperature, b) outdoors, and c) ambient laboratory relative humidity and temperature, with the latter exhibiting the longest times-to-corrosion. Chloride threshold for the 40^{o}C and b) condition exposures exceeded those for the ambient laboratory and outdoor exposures by a factor of two.

6. Time-to-corrosion initiation was less by 50 percent for the present HA G109 specimens and by a factor of four for the LA ones compared to times for a previous set of exposures. This may have been a consequence of differences in concrete moisture between the two sets.

7. An analysis of air voids along the top of the upper rebar trace indicated that corrosion initiated preferentially at the larger of these (maximum void diameter was 5 mm). This effect was more pronounced for the a) HA compared to LA specimens because the former exhibited a higher density and larger size of voids and b) wire brushed compared to as-received bar surface condition.

8. In G109 specimens of variable size (2X, 4X, and 8X compared to the standard), corrosion initiated after a shorter exposure time the greater the number of bars (alternatively, the greater the bar surface area). This is consistent with an increased probability that a significant compositional or microstructural feature was present the greater the number of bars or bar surface area. Such statistical effects are important in extending results from relatively small laboratory

specimens to actual structures, as illustrated also by the chloride threshold data (see Conclusion 4).

9. Time-to-corrosion for piling type specimens exposed to a cyclic water level that simulated tidal action was less than when water level was constant.

10. Time-to-corrosion for w/c 0.50 HA piling specimens exceeded that for w/c 0.50 LA ones by a factor of approximately 2.5. For comparable w/c 0.37 ones this difference was by a factor of two.

The following conclusions were reached from experiments wherein concrete specimens were subjected to 1) periodic spraying with a NaCl solution while exposed to constant relative humidity, RH (RH = 35, 55, 75, and 95 percent), and 2) continuous ponding with a NaCl solution while exposed at ambient temperature (~23°C) and in constant temperature chambers at 0, 30, and 40°C:

1. The effective diffusion coefficient, D_{eff}, increased with increasing RH. Also, the value of D_{eff} for a specimen that was cycled between RH 35 and 95 was approximately the same as for the average of these two values (RH = 65 percent). Thus, variations in RH, as invariably occur in outdoor exposures, apparently did not affect Cl^- intrusion rate.

2. The effective diffusion coefficient, D_{eff}, increased with increasing temperature. Also, D_{eff} was greater for a specimen that was cycled between 20 and 40°C than for one constantly exposed at 40°C. This indicates that caution should be exercised in projecting Cl^- intrusion rates in actual service from laboratory experiments performed at constant temperature.

RECOMMENDATIONS

1. Continued research effort should focus on the utility of high alkalinity cements for providing concrete structures with enhanced resistance to salt water induced reinforcement corrosion. Apparently, these cements provide an increase in time-to-corrosion of 2-10 times compared to that of concretes that utilize normal alkalinity cements (Na_2O_e < 0.60) at no additional cost.

2. Additional experiments should be performed to confirm that the effective diffusion coefficient of chlorides in concrete becomes elevated upon thermal cycling compared to when temperature is constant.

3. The role of air voids and, presumably, entrapped air in providing corrosion initiation sites should be further characterized and quantified.

BIBLIOGRAPHY

[1] Spellman, D.S. and Stratfull, R.F., "Concrete Variables and Corrosion Testing," *Highway Research Record*, No. 423, 1963, p. 27.

[2] Clear, K.C., "Time-to-Corrosion of Reinforcing Steel in Concrete Slabs," Report No. FHWA-RD-76-70, Federal Highway Administration, Washington, D.C., 1976.

[3] Hausmann, D.A., *Materials Protection*, Vol. 6(10), 1967, p. 23.

[4] Gouda, V.K., *British Corrosion Journal*, Vol. 5, 1970, p. 198.

[5] Hausmann, D.A., *Materials Performance*, Vol. 37(10), 1998, p. 64.

[6] Breit, W., *Mater. Corrosion*, Vol. 49, 1998, p. 539.

[7] Charvin, S., Hartt, W.H., and Lee, S. K., "Influence of Permeability Reducing and Corrosion Inhibiting Admixtures in Concrete upon Initiation of Salt Induced Embedded Steel Corrosion," paper no. 00802 presented at CORROSION/00, March 26-31, 2000, Orlando.

[8] Li, L. and Sagüés, A.A., *Corrosion*, Vol. 57, 2001, p. 19.

[9] Glass, G.K. and Buenfeld, N.R., "Chloride Threshold Levels for Corrosion Induced Deterioration of Steel in Concrete," paper no. 3 presented at RILEM International Workshop on Chloride Penetration into Concrete, Oct. 15-18, 1995, Saint Rémy-les-Chevreuse.

[10] Broomfield, J.P., *Corrosion of Steel in Concrete*, E&FN Spon, London, 1997, pp. 22-25.

[11] Bentur, A., Diamond, S, and Berke, N.S., *Steel Corrosion in Concrete*, E&FN Spon, London, 1997, pp. 15,16.

[12] Tutti, K., *Corrosion of Steel in Concrete*, Report No. Fo 4, Swedish Cement and Concrete Research Institute, Stockholm, 1982.

[13] Longuet, P., Burglen, L., and Zelwer, A., *Rev. Matér.*, Vol. 35, 1973, p. 676.

[14] Barneyback, R.S. and Diamond, S., *Cem. Concr. Res.*, Vol. 11, 1982, p. 279.

[15] Page, C.L. and Vennesland, O., *Mater. Struct*., Vol. 19, 1983, p. 16.

[16] Sagüés, A.A., Moreno, E.I., and Andrade, C., *Cem. Concr. Res*., Vol. 27, 1997, p. 1747.

[17] Li, L., Sagüés, A.A., and Poor, N, *Cem. Concr. Res*., Vol. 29, 1999, p. 315.

[18] Hartt, W.H., Charvin, S., and Lee, S.K., "Influence of Permaeability Reducing and Corrosion Inhibiting Admixtures in Concrete upon Initiation of Salt Induced Embedded Metal Corrosion," final report submitted to FDOT by FAU on Project WPI 0510716, June 18, 1999.

[19] Li, l., Nam, J., and Hartt, W.H., "Ex-Situ Leaching Measurement of Concrete Alkalinity," submitted to Cement and Concrete Research.

[20] Bamforth, P.B., "Definition of Exposure Classes and Concrete Mix Requirements for Chloride Contaminated Environments," *Corrosion of Reinforcement in Concrete*, Eds: Page, C.L., Treadaway, K.W.J., and Bamforth, P.B., Soc. Chem. Ind., London, 1996, p. 176.

[21] Bamforth, P.B. and Price, W.F., "Factors Influencing Chloride Ingress into Marine Structures," *Concrete 2000*, Eds: Dhir, R.K. and Jones, M.R., E&FN Spon, London, 1993, p. 1105.

[22] Hartt, W.H., Nam, J, and Li, L., "Critical Issues Related to Corrosion Induced Deterioration Projection for Concrete marine Bridge Substructures," Final Report submitted to Florida Department of Transportation on Project BD776, December 30, 2003.

[23] J. Nam, J., W.H. Hartt, K. Kim, and L. Li, "Effect of Cement Alkalinity upon Time-to-Corrosion of Reinforcing Steel in Concrete undergoing Chloride Exposure," paper no. 03290 to be presented at CORROSION/03, San Diego, March 17-21, 2003, San Diego.

[24] ASTM Standard Test Method G 109-99, "Determining the Effect of Chemical Admixtures on the Corrosion of Embedded Steel Reinforcement in Concrete Exposed to Chloride Environments," Annual Book of ASTM Standards, Vol. 03.02, American Society for Testing and Materials, 100 Barr Harbor Drive, West Conshohocken, PA.

[25] Hausmann, D.A., *Materials Protection*, Vol. 6(10), 1967, p. 23.

[26] Gouda, V.K., *British Corrosion Journal*, Vol. 5, 1970, p. 198.

[27] Hausmann, D.A., *Materials Performance*, Vol. 37(10), 1998, p. 64.

[28] Breit, W., *Mater. Corrosion*, Vol. 49, 1998, p. 539.

[29] Li, L. and Sagüés, A.A., *Corrosion*, Vol. 57, 2001, p. 19.

[30] Diamond, S., *Cement and Concrete Research*, Vol. 11 (3), 1981, p. 383.

[31] Diamond, S., "Effects of Microsilica (Silica Fume) on Pore-Solution Chemistry of Cement Pastes", *Communications of American Ceramic Society*, May, 1983, p. C82.

[32] Arya, C and Xu, Y., *Cement and Concrete Research*, Vol. 25, 1995, p. 893.

[33] Page, C.L. and Vennesland, O., *Mater. Struct*., Vol. 16, 1983, p. 19.

[34] Constantiner, D. and Diamond, S., "Pore solution analysis: Are There Pressure Effects?," in "*Mechanisms of Chemical Degradation of Cement-based Systems"*, Eds.: Scrivener, K.L. and Young, J.F., E & FN SPON, London, 1997, p. 22.

[35] Tritthart, J., *Cement and Concrete Research*, Vol. 19, 1989, p. 683.

[36] Kawamura, M., Kayyali, O.A., and Haque, M.N., *Cement and Concrete Research,* Vol. 18, 1988, 763.

[37] Kayyali, O.A. and Haque, M. N., *Journal of Materials in Civil Engineering*, Vol. 2, 1990, p. 24.

[38] Larbi, J.A., Fraay, A.L.A., and Bijen, J. L., *Cement and Concrete Research*, Vol. 20, 1990), p. 506.

[39] Duchesne, J. and Berube, M.A., *Cement and Concrete Research*, Vol. 24, 1994, 456.

[40] "Florida Method of Test for Determining Low-Levels of Chloride in Concrete and Raw Materials," Designation FM 5-516, Florida Department of Transportation, Tallahassee, FL, Sept., 1994.